

Click-Capable Phenanthriplatin Derivatives as Tools to Study Pt(II)-Induced Nucleolar Stress

Paul D. O'Dowd,^{a,b,‡} Andres S. Guerrero,^{c,‡} Hannah C. Pigg,^c Katelyn R. Alley,^c Fiona O'Neill,^d Justine Meiller,^d Chloe Hobbs,^a Daniel A. Rodrigues,^a Brendan Twamley,^e Finbarr O'Sullivan,^d Victoria J. DeRose,^c Darren M. Griffith^{*a,b}.

^a Department of Chemistry, Royal College of Surgeons in Ireland, Dublin, Ireland

^b SSPC, the Science Foundation Ireland Research Centre for Pharmaceuticals

^c Department of Chemistry and Biochemistry, University of Oregon, Eugene, OR, USA

^d Life Science Institute, Dublin City University, Dublin, Ireland.

^e Department of Chemistry, Trinity College Dublin, Dublin, Ireland.

Platinum, anticancer, phenanthriplatin, click chemistry, nucleolar stress

ABSTRACT: It is well-established that oxaliplatin, one of the three Pt(II) anticancer drugs approved worldwide, and phenanthriplatin, an important preclinical monofunctional Pt(II) anticancer drug, possess a different mode of action to that of cisplatin and carboplatin, namely the induction of nucleolar stress. The exact mechanisms that lead to Pt-induced nucleolar stress are however still poorly understood. As such, studies aimed at better understanding the biological targets of both oxaliplatin and phenanthriplatin are urgently needed to expand our understanding of Pt-induced nucleolar stress and guide the future design of Pt chemotherapeutics. One approach which has seen great success in the past, is the use of Pt-click complexes to study the biological targets of Pt drugs. Herein, we report the synthesis and characterization of the first examples of click-capable phenanthriplatin complexes. Furthermore, through monitoring the relocalization of nucleolar proteins and the DNA damage repair biomarker γ H2AX, and by investigating their *in vitro* cytotoxicity we show that these complexes successfully mimic the cellular responses observed for phenanthriplatin treatment in the same experiments. The click-capable phenanthriplatin derivatives described here expand the existing library of Pt-click complexes. Significantly they are suitable for studying nucleolar stress mechanisms and further elucidating the biological targets of Pt complexes.

INTRODUCTION

There are three platinum (Pt) complexes approved worldwide for treating cancer; cisplatin, carboplatin and oxaliplatin. Together these drugs play an important role in cancer treatment, with central roles in the treatment of testicular, ovarian, bladder and colorectal cancers.^{1, 2} Despite this, the clinical use of Pt agents is commonly hampered by toxic side effects and the development of drug resistance. As such, much research has focused on the design of novel Pt(II) complexes with improved activity, reduced adverse effects and an ability to overcome Pt-resistance mechanisms.^{3, 4} One such complex designed under this premise is phenanthriplatin.⁵

Phenanthriplatin is a monofunctional cisplatin derivative which has increased cellular uptake and has been shown to be 7-40 times more effective than cisplatin against a wide range of cancer cell lines. Moreover, phenanthriplatin's spectrum of activity is different to that of the approved Pt chemotherapeutics.^{5, 6} Unlike the FDA-approved Pt drugs, phenanthriplatin treatment primarily results in the formation of monoadducts with DNA. The formation of these adducts is believed to occur following an initial intercalation step of the phenanthridine ligand between DNA bases, followed by the formation of a Pt-nucleobase DNA monoadduct.⁷⁻¹⁰ Phenanthriplatin-DNA monoadducts have been shown to inhibit RNA polymerase II though they can still be bypassed by DNA polymerase η .^{11, 12} Furthermore phenanthriplatin has also been shown to be an effective topoisomerase II poison.¹³

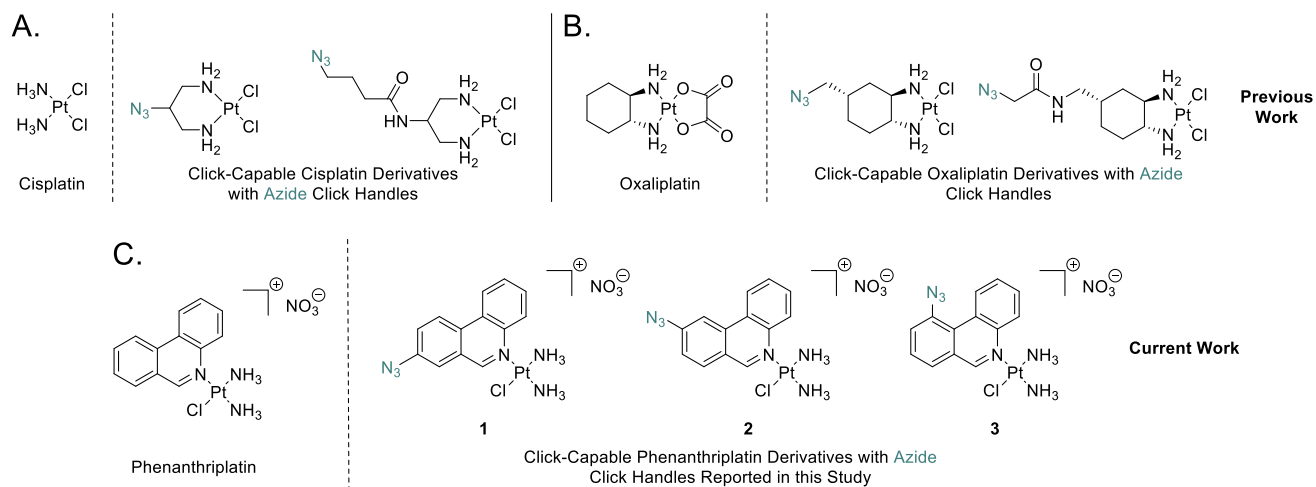


Figure 1. A. Structures of select previously reported azide-containing cisplatin click-derivatives.^{14, 15} B. Structures of previously reported azide-containing oxaliplatin click-derivatives.¹⁶ C. Structures of click-capable azide-containing phenanthriplatin-derivatives reported in this study.

Interestingly, while the DNA-binding properties of phenanthriplatin are well studied, a recent study identified that the primary mechanism of action (MOA) of phenanthriplatin and oxaliplatin is associated with their ability to induce nucleolar stress¹⁷. In the same study the MOA of cisplatin and carboplatin were linked with classical DNA damage response (DDR).¹⁷ Nucleolar stress is a term used to describe events which disturb normal ribosome biogenesis, which can ultimately lead to cell apoptosis.¹⁸ Much research has subsequently been carried out to better understand the nucleolar stress response following oxaliplatin administration.¹⁹⁻²⁵ In the case of phenanthriplatin however, reports remain limited, with the biological pathways activated by the drug still poorly understood.

A previous study has indicated that phenanthriplatin's capacity to induce nucleolar stress may be dependent on the number of aromatic rings present in the phenanthridine ligand. Indeed, other monofunctional Pt complexes based on isoquinoline and pyridine, for example, do not induce nucleolar stress responses.²⁶ More recently, a monoadduct-generating ruthenium (Ru) complex has also been reported to induce nucleolar stress with a similar biological phenotype to phenanthriplatin.²⁷ Given the structural differences between oxaliplatin, phenanthriplatin and the recently reported octahedral Ru complex, it is clear that nucleolar stress can be initiated despite differences in the nature of ligands and metal centers of anticancer agents. As such, the molecular events leading to nucleolar stress induction may also differ between the complexes. Given these observations and that Pt-induced nucleolar stress is poorly understood, probes to study the molecular targets of phenanthriplatin are of great importance.

One approach which has previously shown great success in identifying the biological targets of Pt-agents is the use of click-capable Pt complexes.^{28, 29} The use of cisplatin-like Pt-click complexes for instance has been successfully employed to identify Pt(II)-DNA, -RNA and -protein adducts in biological media, cell extracts and yeast cells, (Figure 1. A.).^{15, 30-34} Recently, our groups reported the first examples of oxaliplatin click complexes and showed one of these derivatives could successfully induce nucleolar stress, (Figure 1. B).¹⁶ To further expand the range of Pt-click complexes available, and to generate a probe that can be used to study potential differences between oxaliplatin- and phenanthriplatin-induced nucleolar stress, we set out to design phenanthriplatin click complexes capable of inducing nucleolar stress responses.

Herein we report the synthesis and characterization of the first examples of phenanthriplatin click complexes, 1-3, (Figure 1. C). Through monitoring the redistribution of nucleolar proteins and biomarkers of DDR, we show that 1-3 successfully mimic the biological effects of the parent complex, and induce nucleolar stress responses. Furthermore, we show that all of the novel complexes can be functionalized by strain-promoted azide-alkyne click reactions following binding to DNA *in vitro*. Finally, we show that 3 exhibits a similar cytotoxicity profile to that of phenanthriplatin against a range of cancer cell lines. As such, we present 1-3 as important tools for studying Pt-induced nucleolar stress alongside recently reported oxaliplatin click complexes.

RESULTS AND DISCUSSION

Synthesis and Characterization.

Previous work has shown that the ability of monofunctional platinum complexes to induce nucleolar stress may be dependent on the size of aromatic ring system attached to the nitrogen donor ligand.²⁶ Despite this we hypothesized that small modifications to the phenanthridine ring system of phenanthriplatin would be possible, without altering the biological activity of the parent complex. Azide click handles have previously been employed in click-capable Pt(II) complexes as the azide group is a small reactive handle and is highly selective for alkyne click partners via Cu (I)-catalyzed azide-alkyne cycloaddition (CuAAC) and strain-promoted azide-alkyne cycloaddition (SPAAC).²⁸ Given the lack of reports describing the effect of small modifications on the activity of phenanthriplatin, modifications at three different positions on the phenanthridine ring were explored. Synthesis of the novel phenanthridine ligands, incorporating the azide group at the 8-, 9- and 10-positions, were carried out in three analogous steps from commercially available starting materials, (Fig. 2). Briefly, an initial Suzuki Reaction coupled with a condensation reaction, led to formation of the phenanthridine ring system. Subsequent reduction of the nitro functional group and conversion of the resulting amine to an azide via a diazonium salt, led to the formation of the desired ligands. Following isolation of the respective ligands, 1-3 were synthesized through reaction with cisplatin and silver nitrate in a similar manner to that reported for phenanthriplatin.⁵ The identity and purity of all complexes were subsequently confirmed by NMR and HRMS analysis.

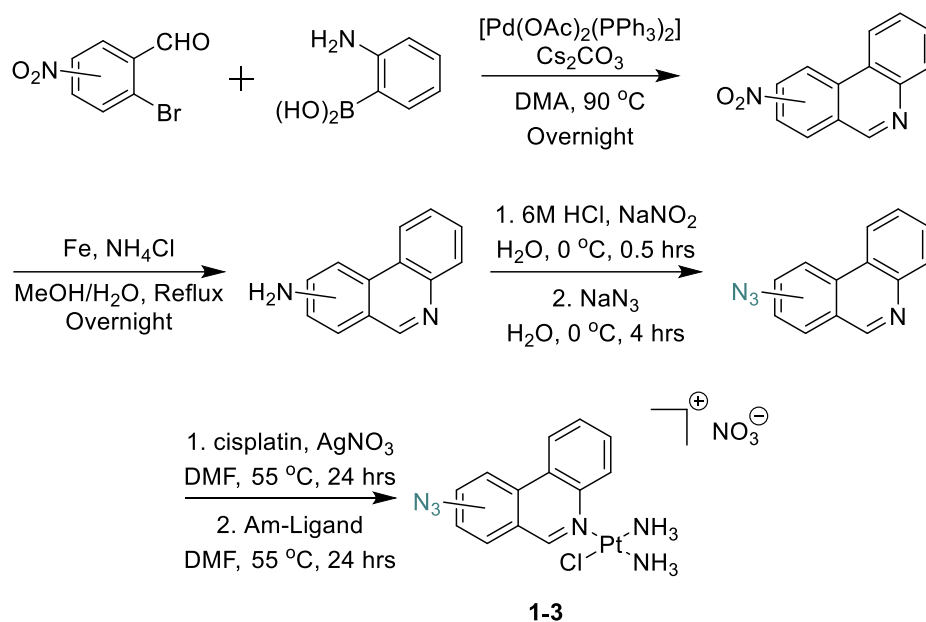


Figure 2. General synthetic pathway for the synthesis of **1-3**

The X-ray crystal structure of **1** was determined, showing successful coordination of the modified phenanthridine ligand to platinum and the desired nitrate-counterion (Fig. 3). In our case, the complex crystallizes as a methanol solvate (Fig. 3). The structure of **1** is similar to the original phenanthriplatin,⁵ and displays expected bond lengths and angles (see Table S4). **1** also crystallizes in a centrosymmetric space group, indicating that it is also a racemate. One notable difference is the angle of the plane normal between the phenanthridine and a line joining the pyridyl nitrogen, the Pt atom and the trans amine nitrogen, $90.92(6)^\circ$. In the nitrate salt of phenanthriplatin, this is $68.29(4)^\circ$ and in the triflate salt of phenanthriplatin,³⁵ $79.15(9)^\circ$ (see Fig. S16). This bending of the phenanthridine moiety with respect to the coordination plane has been attributed to packing forces. In **1**, there are significantly more π - π interactions which align the phenanthridine moieties into stacks parallel to the b-axis (see Fig. S17). As the coordination environment around the metal center has not changed, the steric protection provided by the phenanthridine in **1** is comparable to phenanthriplatin (1 , C3-Pt1, $3.184(4)$ Å; phenanthriplatin, $3.220(8)$ Å).

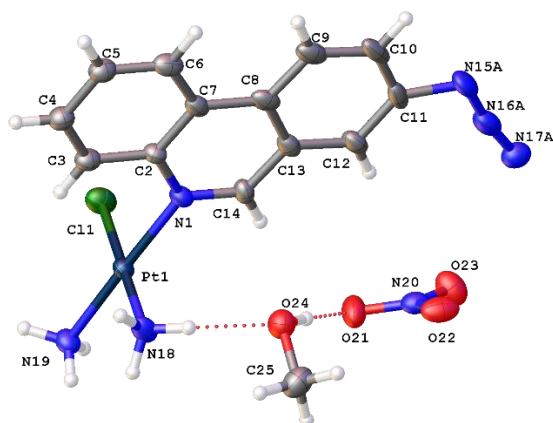


Figure 3. X-ray structure of **1**, showing the majority occupied azide moiety (75%) only. Methanol solvate hydrogen bonded to both NH_3 and NO_3^- groups. Displacement parameters shown at 50% probability.

1-3 induce nucleolar protein redistribution to a similar degree as phenanthriplatin.

Following synthesis of **1-3** we turned our attention to investigate whether the novel complexes could induce nucleolar stress in a similar fashion to the parent complex, phenanthriplatin. One hallmark of nucleolar stress is the relocation of the nucleolar protein nucleophosmin (NPM1). In non-drug

treated cells, NPM1 is found in well-defined regions within the granular region of the nucleolus, however following induction of nucleolar stress, the protein redistributes throughout the nucleoplasm.¹⁸

Through immunofluorescence staining techniques, the distribution of NPM1 in A549 cells was quantified by the coefficient of variation (CV, see Methods). As previously reported, CV values of ~ 0.6 are indicative of cells undergoing nucleolar stress, while CV values ~ 1.0 indicate a lack of stress.²⁰ Immunofluorescence levels of NPM1 were quantified 24 hr following treatment with 1-3 at 0.5 μ M, as previous studies have indicated that treatment with phenanthriplatin at this concentration results in a strong nucleolar stress response.²⁶ Actinomycin D (ActD) a FDA approved anticancer drug known to induce nucleolar stress was included in this study alongside known Pt nucleolar stress inducers, oxaliplatin and phenanthriplatin.²⁴

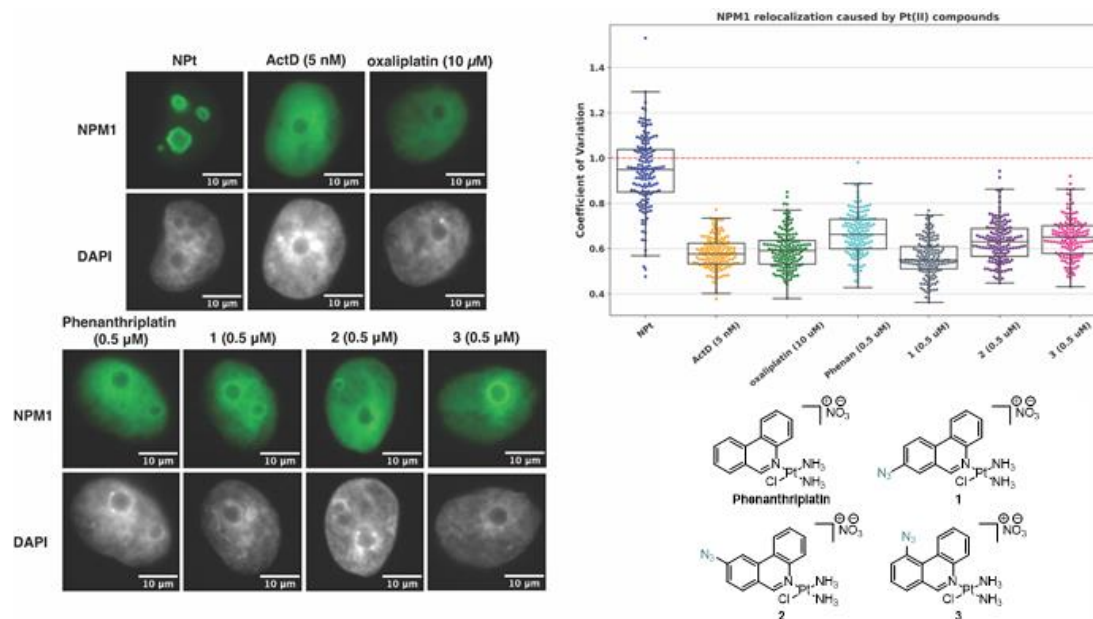


Figure 4. Visualization and quantification of NPM1 relocation (NPM1: green, DAPI: gray) induced by 1-3. Treatment conditions indicated (5 nM for ActD, 10 μ M for oxaliplatin and 0.5 μ M for phenanthriplatin and 1-3) in A549 cells at 24 hrs treatment. Representative images and CV calculations based on 3 trials are shown. Full cell images found in ESL,† Fig. S1. For each treatment data set, boxes represent median, first and third quartiles, and vertical lines are the range of data with outliers (see Experimental Section). Scale bar = 10 μ m.

Following treatment with 1-3, pronounced redistribution of NPM1 throughout the nucleoplasm was observed, (Fig. 4). Importantly, the degree of redistribution of NPM1 remained similar following treatment with each of 1-3 (~ 0.6). Furthermore, 1-3 were found to induce a similar degree of NPM1 redistribution as the known nucleolar stress inducers ActD, oxaliplatin and phenanthriplatin.

Redistribution of the nucleolar protein fibrillarin (FBL) is another hallmark of nucleolar stress responses.^{21, 24} FBL is normally found in the dense fibrillary component of nucleoli, however upon nucleolar stress FBL condenses in nucleolar cap-like structures.³⁶ Using a FBL immunofluorescence assay, FBL localization in the nucleolus was observed following treatment with ActD, oxaliplatin and phenanthriplatin. Importantly, while FBL nucleolar cap formation has previously been reported following treatment with oxaliplatin, FBL distribution has not been monitored following treatment with phenanthriplatin to the best of our knowledge. As expected however, treatment with phenanthriplatin at clinically relevant concentrations resulted in nucleolar cap formation, in a similar manner to ActD and oxaliplatin, (Fig. 5). In contrast, FBL distribution following treatment with cisplatin, remained relatively unchanged, (Fig. 5). This highlights the potential difference in MOA of cisplatin and the nucleolar stress-inducing Pt(II) drugs. In a similar manner to phenanthriplatin, pronounced FBL nucleolar caps were observed following treatment of A549 cells with 1-3 for 24 hrs, (Fig. 5).

Taken together, results from the NPM1 and FBL immunofluorescence assays indicate that treatment with complexes 1-3 result in nucleolar protein redistribution, and thus nucleolar stress responses, to a similar degree as phenanthriplatin. Additionally, these complexes appear equally effective at induc-

ing nucleolar stress regardless of the position of the azide substituent. This suggests small modifications to phenanthriplatin's aromatic nitrogen donor ligand are tolerated in all three of the positions functionalized in this study.

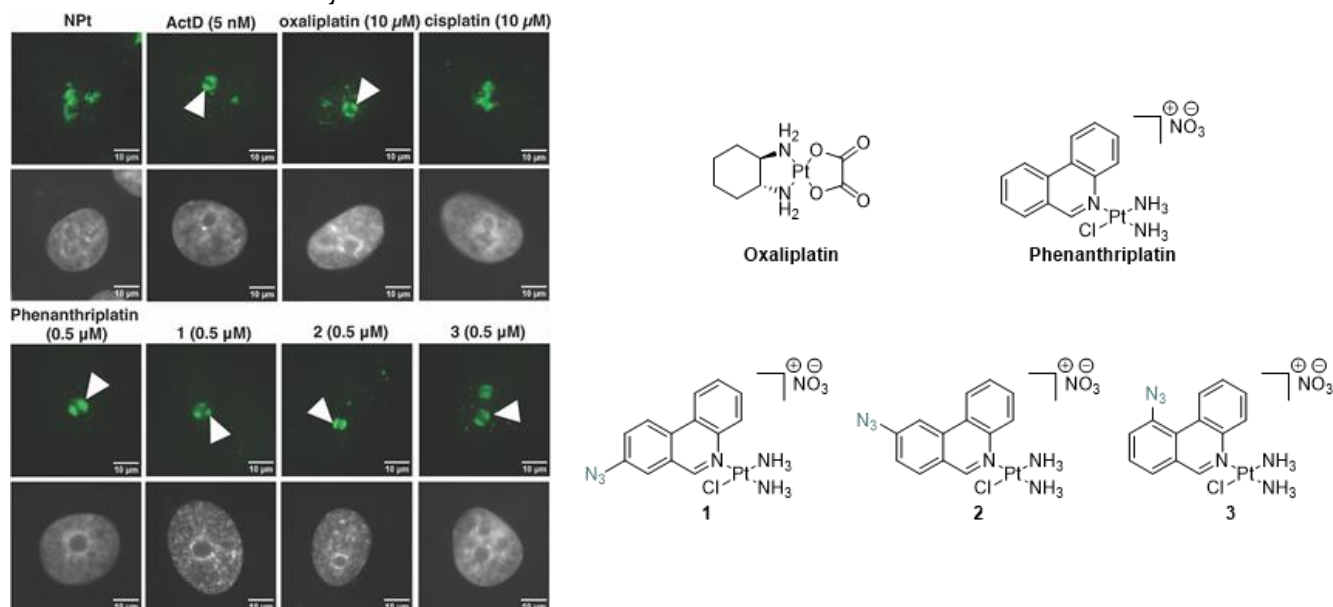


Figure 5. Nucleolar morphological changes monitored by fibrillar staining (fibrillar staining: green, DAPI: gray). Treatment conditions at 5 nM for ActD, 10 μM for oxaliplatin and 0.5 μM for phenanthriplatin and **1-3** in A549 cells at 24 hrs treatment. Nucleolar cap formation is indicated by a white arrow. Scale bar = 10 μm.

γH2AX levels following treatment with **1-3** are similar to phenanthriplatin

Nucleolar stress can occur as an independent stress response or as a downstream effect of DDR.³⁷ H2AX phosphorylation plays a crucial role in recruiting DNA damage repair proteins and as such is commonly used as an indirect marker of DDR.¹⁷ As such, to examine whether the redistribution of NPM1 and FBL observed following treatment with **1-3** is due to an independent nucleolar stress response, levels of γH2AX were monitored following treatment with **1-3**.

In these experiments, γH2AX levels were monitored 24 hrs after treatment by quantifying immunofluorescence intensities, with results reported as % of nuclei positive for γH2AX (see Experimental Section). In line with previous results, treatment of A549 cells with the known DDR inducer, cisplatin, resulted in a strong γH2AX response indicating activation of DNA damage repair pathways, (Fig. 6).¹⁶

21

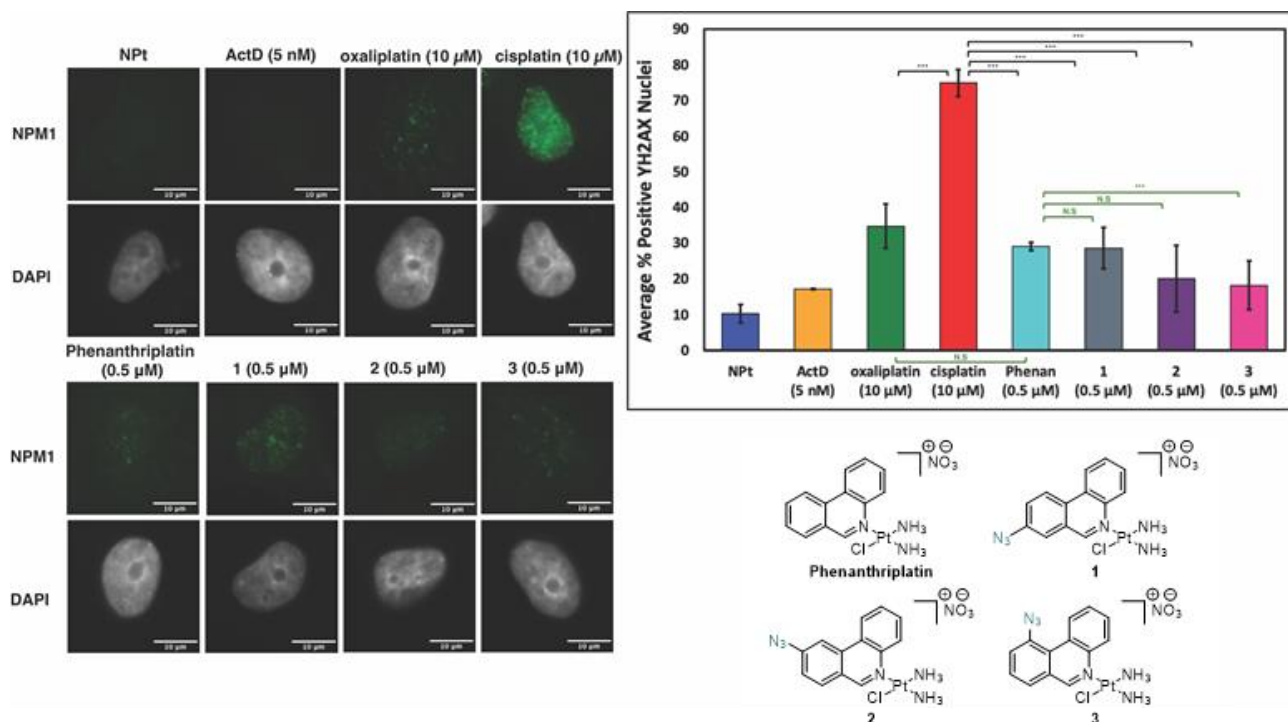


Figure 6. Visualization and quantification of γ H2AX (γ H2AX: green, DAPI: gray) as an indicator of DDR induced by 1-3. Treatment conditions indicated (5 nM for ActD, 10 μ M for oxaliplatin and cisplatin, and 0.5 μ M for phenanthriplatin and 1-3) in A549 cells at 24 hrs treatment; average of 3 trials and std; quantification performed described in Experimental Section. Scale bar = 10 μ m. *** $p < 0.05$, N.S. $p > 0.05$.

Compared to cisplatin, treatment with known nucleolar stress inducers ActD and oxaliplatin both resulted in lower levels of γ H2AX ($p < 0.05$), in agreement with previous studies, (Fig. 6).^{16, 21} Furthermore, γ H2AX levels following treatment with phenanthriplatin were also significantly lower than observed following treatment with cisplatin, ($p < 0.05$), (Fig. 6). These results further emphasize the likely differences in mechanism of action following treatment with the different classes of Pt-agents.

Similarly, to the known inducers of nucleolar stress, treatment with 1-3 was also found to result in significantly lower levels of γ H2AX than cisplatin treatment ($p < 0.05$), (Fig. 6). Moreover, γ H2AX levels following treatment with 1, 2 or 3 were found to be similar or lower than those following phenanthriplatin administration. Together these results indicate that treatment with 1, 2 and 3 cause similar γ H2AX levels to phenanthriplatin, and a less pronounced DDR than cisplatin. This result supports an independent nucleolar stress response following treatment with 1-3. It is worth mentioning however, that in the case of oxaliplatin, inhibition of two DDR signaling kinases, ATM and ATR, have recently been reported to result in partial protection from nucleolar stress responses.²⁵ This partial protection is observed despite low levels of H2AX phosphorylation following treatment with oxaliplatin (Fig. 6).^{16, 21} This indicates that further studies with phenanthriplatin, and indeed 1-3, are likely needed to fully elucidate the role of DDR in the nucleolar response of phenanthriplatin.

1-3 successfully bind hairpin DNA *in-vitro* and can be functionalized by strain-promoted azide-alkyne click chemistry.

It has previously been reported that intercalation of the phenanthridine ring of phenanthriplatin with DNA plays an important role in the formation of Pt-DNA adducts.⁷⁻¹⁰ As such, modifications to the phenanthridine ring of phenanthriplatin may result in impaired DNA intercalation and Pt-DNA adduct formation. Additionally, intercalation of the azide-modified complexes 1-3, could result in steric hindrance that prevents efficient click-functionalization following biomolecular interactions.

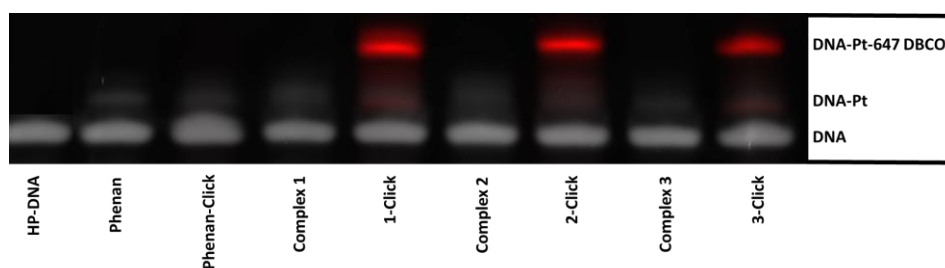


Figure 7. dPAGE analysis of Pt(II) complexes incubated with HP DNA. Complexes labeled as “click” were first incubated with HP for 24 hrs followed by a click reaction with Alexa-647 DBCO for an additional 24 hrs, giving a total DNA incubation time of 48 hrs. Control complexes were incubated for 48 hrs with HP with no click reaction. All samples were purified by spin column before analysis by dPAGE. Grey: DNA stained with SYBR gold (539 nm emission wavelength), red: DNA-Pt-647 DBCO complex (671 emission wavelength).

To test the DNA-binding capability of 1, 2 and 3, the complexes were incubated alongside phenanthriplatin, with a 20-nucleotide DNA hairpin (HP) containing a single GG site. Following incubation, 1, 2 and 3 showed similar Pt-DNA adduct formation to phenanthriplatin as measured by dPAGE, (Fig. 7). This indicates that the small azide modification present in 1-3 does not prevent the complexes from binding to DNA *in-vitro*. Following initial incubation of the complexes with HP-DNA, a strain-promoted azide-alkyne click reaction was carried out with the click-capable fluorophore, Alexa-647 DBCO.^{16, 38} Subsequent analysis by fluorescence imaging, showed successful strain-promoted azide-alkyne click reaction in the case of each of 1, 2 and 3, indicating the complexes can be successfully modified following reaction with biomolecules, (Fig. 7). Taken together, these results indicate that 1, 2 and 3 are suitable click-mimics of phenanthriplatin and are suitable derivatives for studying Pt-modified biomolecules.

In-vitro cytotoxicity of 3 is similar to phenanthriplatin across a range of cancer cell lines.

Given the similar activity of 1, 2 and 3 in the prior experiments undertaken, 3 was chosen as a representative example for further study. The *in vitro* cytotoxicity of 3, phenanthriplatin, oxaliplatin and cisplatin were investigated against a range of cancer cell lines after 6 days treatment.

Table 1. IC₅₀ values for 3, phenanthriplatin, oxaliplatin and cisplatin at 6 days, as determined by acid phosphatase assay

IC ₅₀ (μM)	3	Phenanthriplatin	Oxaliplatin	Cisplatin
A549	0.203 ± 0.023	0.201 ± 0.022	1.725 ± 0.434	2.096 ± 0.441
PANC-1	0.092 ± 0.021	0.096 ± 0.025	4.389 ± 0.943	3.794 ± 0.837
SK-LU-1	0.211 ± 0.022	0.327 ± 0.032	2.806 ± 0.582	0.659 ± 0.198

In line with the results obtained for nucleolar protein redistribution and γH2AX levels, 3 was found to exhibit similar *in vitro* cytotoxic activity to phenanthriplatin against all the cancer cell lines investigated; A549 (non small cell lung), PANC-1 (pancreatic) and SK-LU-1 (lung) cell lines. Previous studies have shown that phenanthriplatin is highly effective against a range of lung and pancreatic cancer cell lines.^{5, 27} These results indicate that cellular processing of 3 and the mechanisms of action activated by the complex, ultimately lead to similar *in vitro* cytotoxic activity as the parent complex.

CONCLUSION

We have reported the design, synthesis and characterization of 1-3, the first azide-containing phenanthriplatin derivatives reported to date. Through monitoring NPM1 localization and FBL cap formation, we have shown that each of the three complexes induce redistribution of nucleolar proteins and disruption to nucleolar morphology to a similar degree as phenanthriplatin. Furthermore, through monitoring γH2AX phosphorylation levels following treatment with 1-3, we have shown that these complexes induce a similar level of DDR activation to phenanthriplatin. Through *in-vitro* DNA hairpin incubation, we have shown that 1-3 can successfully form adducts with DNA and can subsequently be functionalized with a fluorescent reporter through strain-promoted azide-alkyne click-

chemistry. Finally, the cytotoxicity of **3** was shown to be similar to phenanthriplatin in a range of cancer cell lines, emphasizing the similarity between the reported click-capable phenanthriplatin mimic and the parent complex, phenanthriplatin. As such, we present **1-3** as suitable click-capable phenanthriplatin mimics for future studies focused on Pt-induced nucleolar stress and better understanding Pt-based cell death pathways.

Cell Culture and Treatment

A549 human lung carcinoma cells (#CCL-185, American Type Culture Collection) were cultured in 5% CO₂ at 37 °C in Dulbecco's Modified Eagle Medium (DMEM) with 10% Fetal Bovine Serum (FBS) and 1% antibiotic-antimycotic. Treatments were performed on cells that had been grown for 11-26 passages to 70% confluency. All treatments were performed for 24 hours at 10 μM for oxaliplatin, 0.5 μM concentrations for phenanthriplatin, **1**, **2**, and **3**. Oxaliplatin was made in a 5 mM stock solution, while phenanthriplatin, **1**, **2**, and **3** was made into a 5 mM stock solution and further diluted to a 250 μM stock solution. The complex stock solutions were made with DMF (phenanthriplatin, **1**, **2**, and **3**), water (oxaliplatin), or DMSO (ActD). Stock solutions were diluted into media immediately prior to drug treatment. Treatments were performed in triplicate and additional replicates are available from the corresponding author upon reasonable request.

Immunofluorescence

Cells were grown on coverslips (Ted Pella product no. 260368, round glass coverslips, 10 mm diam. 0.16–0.19 mm thick) as described above. After treatment was complete, cells were washed with phosphate buffered saline (PBS) and fixed with 4 % paraformaldehyde (PFA) in PBS for 20 minutes at room temperature. PFA was removed using aspiration and cells were permeabilized with 0.5 % Triton-X in PBS for 20 minutes at room temperature. Two ten-minute blocking steps were then performed with 1 % bovine serum albumin (BSA) in PBST (PBS with 0.1 % Tween-20). Cells were incubated for one hour in primary antibody NPM1 or γH2AX for DDR and for an hour and a half with the primary antibody Fibrillarin for nucleolar stress response (NPM1 monoclonal antibody, FC-61991, ThermoFisher, 1 : 800 dilution in PBST with 1 % BSA) (Phospho-Histone H2A.X (Ser139) Monoclonal Antibody (CR55T33, ThermoFisher, 2.5 μg in PBST with 1% BSA), (anti-Fibrillarin antibody ab4566 from Abcam, 1:400 dilution) and 1 hour in secondary antibody for NPM1 or γH2AX and an 1.5 hrs for fibrillarin (Goat Anti-Mouse IGG H&L Alexa Fluor® 488, ab150113, Abcam, 1 : 1000 dilution in PBST with 1 % BSA), with three 5 minute wash steps using PBST between antibody incubations. Washed again in the same manner before mounting the slides. Coverslips were then mounted on slides with ProLong™ Diamond Antifade Mountant with DAPI (ThermoFisher) according to manufacturer's instructions.

Image Processing and Quantification

The quantification of NPM1 relocalization was performed in an automated fashion using a Python 3 script. Images were preprocessed in ImageJ,^{39, 40} to convert the DAPI and NPM1 channels into separate 16-bit grayscale images. Between 50-250 cells were analyzed for each treatment group. Nuclei were segmented using the DAPI images using Li thresholding function in the Scikit-Image Python package.⁴¹ The coefficient of variation (CV) for individual nuclei, which is defined as the standard deviation in pixel intensity divided by the mean pixel intensity, was calculated from the NPM1 images using the SciPy Python package. All the data was normalized to the no-treatment in each experiment. NPM1 imaging results for each complex were observed in triplicate. Data are represented as boxplots generated using Seaborn within Python.

Quantification of γH2AX intensity and foci was performed with CellProfiler 4.2.1 software.⁴² In one analysis method, a “percent positive” value was calculated for each treatment condition relative to the untreated control. A threshold was determined for a positive γH2AX result based on the 90th percentile intensity value of the untreated control for each time point. Nuclei in the experimental samples with integrated intensity levels higher than this were counted as positive for γH2AX. Significance testing was done via t-test to obtain a p-value.

In vitro DNA Gel Binding and Fluorophore Clicking

Hairpin DNA sequence (TATGGTATTTTATACCATA) (280 μM) was folded by rapid heating to 90 °C and slow cooling to 4°C in 10 mM Na₂HPO₄/NaH₂PO₄ buffer (pH 7.1), 0.1 M NaNO₃, and 10 mM Mg(NO₃)₂.

The platinum complex (830 μM) was then added and the solution was incubated at 37 °C for 24 hrs. For click complexes, 195 μM of Alexa-657 DBCO (AZDye) was added and incubated 37 °C for an additional 24 hrs. Non-click control complexes were incubated for an additional 24 hrs. at 37 °C. All complexes were then purified with Sephadex G-25 Medium size exclusion resin (GE Healthcare) on laboratory-prepared spin columns (BioRad) to remove unbound platinum and fluorophore. Purified samples were added at a DNA concentration of 200 ng on dPAGE (19:1 20% acrylamide in 8M urea) and ran at 180 V for 2 hours. Gels were then stained with SYBR gold for 5 minutes and imaged using a GE Amersham Typhoon gel imager.

In Vitro proliferation assay

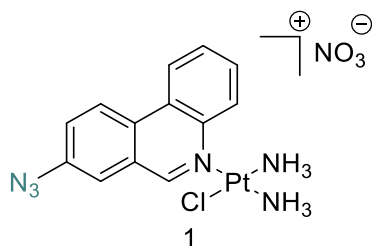
A549, SK-LU-1 (lung adenocarcinoma) and Caco-2 (colorectal adenocarcinoma) cancer cell lines were maintained in RPMI 1640 medium supplemented with 10% fetal bovine serum (PAA Labs, Austria). PANC-1 cells (pancreatic carcinoma) were maintained in Dulbecco's Modified Eagle's medium (DMEM) supplemented with 5% fetal bovine serum (Gibco), 2% L-Glutamine (Sigma, St Louis, MO, USA). All cell lines were kept at 37°C in a 5% CO₂, 95% air humidified incubator. Cells were cultured in 96-well flat-bottomed plates for 24 hours before they were exposed to a range of concentrations of the targeted therapies for 6 days. The cell densities varied from 0.6 $\times 10^4$ cells/ mL (Caco-2) to 1 $\times 10^4$ cells/ mL (A549) and 2 $\times 10^4$ cells/ mL (SK-LU-1 and PANC-1). The percentage cell survival was then determined using an Acid Phosphatase assay. Briefly, media was removed from the plates and each well was washed twice with PBS. The cells were exposed to 10 mM PNP substrate in 0.1M sodium acetate for approximately 1 hour. The reaction was stopped using 1M NaOH and the plates were read at 405 nm and 620 nm on a plate reader. The percentage cell survival was calculated as a percentage relative to a non-treated control.

Synthesis

Oxaliplatin and cisplatin were purchased from TCI. Unless otherwise noted, starting materials were purchased from Millipore Sigma Aldrich, TCI, or BLD Pharm. Phenanthriplatin was synthesized according to previously published methods.⁵

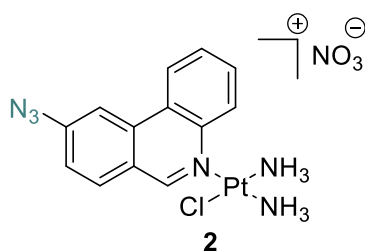
General synthesis of 1-3

AgNO₃ (0.17 g, 1.00 mmol) was added to a solution of cisplatin (0.30 g, 1.00 mmol) in 15 mL DMF. The reaction mixture was then stirred in the dark at 55°C overnight. Following stirring, precipitated AgCl was removed by filtration through celite. Azidophenanthridine (0.20 g, 0.90 mmol) was then added to the filtrate and the reaction mixture stirred for a further 24 hr at 55°C. On returning, the solvent was removed under reduced pressure and the residue resuspended in approx. 30 mL methanol. The mixture was then filtered, and the crude product precipitated by adding 100 mL diethyl ether to the filtrate. The crude product was further purified by redissolving in methanol and recrystallization from a methanol diethyl ether solution. The final compound was isolated by vacuum filtration, washed with diethyl ether and dried under reduced pressure.



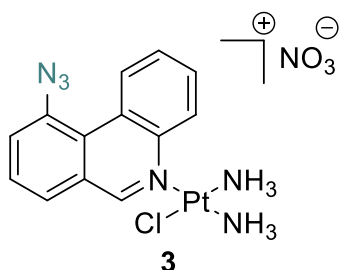
Cis-[Pt(NH₃)₂(8-azidophenanthridine)Cl]NO₃, 1

Yellow crystals were obtained following recrystallization from MeOH/Et₂O (88 mg, 18%). ¹H NMR (400 MHz, DMSO-d₆) δ 9.94 (s, 1H), 9.75 (d, 1H, *J* = 8.3 Hz), 8.99 (d, 1H, *J* = 9.0 Hz), 8.89 (d, 1H, *J* = 8.1 Hz), 8.25 (s, 1H), 8.01 (t, 1H, *J* = 7.5 Hz), 7.90 (m, 2H), 4.56 (s, 3H), 4.44 (s, 3H). ¹³C NMR (101 MHz, MeOD-d₄) δ 160.5, 143.7, 142.4, 130.8, 130.5, 130.4, 130.3, 128.9, 127.2, 126.9, 125.7, 124.0, 118.9. HRMS (ESI+) (MeOH) [M - NO₃]⁺: *m/z* calcd for C₁₃H₁₄ClN₆Pt: 484.0616, found: 484.0624.



Cis-[Pt(NH₃)₂(9-azidophenanthridine)Cl]NO₃, 2

An off-white solid was obtained following recrystallization from MeOH/Et₂O (71 mg, 14%). ¹H NMR (400 MHz, DMSO-*d*₆) δ 9.87 (s, 1H), 9.75 (d, 1H, *J* = 8.4 Hz), 8.96 (d, 1H, *J* = 8.2 Hz), 8.57 (s, 1H), 8.48 (d, 1H, *J* = 8.6 Hz), 8.02 (t, 1H, *J* = 7.6 Hz), 7.88 (t, 1H, *J* = 7.5 Hz), 7.67 (d, 1H, *J* = 8.4 Hz), 4.63 (s, 3H), 4.48 (s, 3H). ¹³C NMR (101 MHz, DMSO-*d*₆) δ 159.1, 145.7, 142.6, 133.4, 132.3, 129.8, 129.2, 128.5, 124.5, 123.8, 123.5, 121.2, 111.7. HRMS (ESI⁺) (MeOH) [M - NO₃]⁺: *m/z* calcd for C₁₃H₁₄ClN₆Pt: 484.0616, found: 484.0627.



Cis-[Pt(NH₃)₂(10-azidophenanthridine)Cl]NO₃, 3

A white solid was obtained following recrystallization from MeOH/Et₂O (122 mg, 25%). ¹H NMR (400 MHz, DMSO-*d*₆) δ 9.95 (s, 1H), 9.89 (dd, 1H, *J* = 8.4, 0.8 Hz), 9.76 (dd, 1H, *J* = 8.5, 0.8 Hz), 8.31 (d, 1H, *J* = 7.1 Hz), 8.12 (dd, 1H, *J* = 7.8, 0.9 Hz), 8.02 (m, 2H), 7.94 – 7.88 (m, 1H), 4.57 (s, 3H), 4.46 (s, 3H). ¹³C NMR (101 MHz, DMSO-*d*₆) δ 153.6, 144.7, 136.3, 129.8, 128.7, 128.3, 128.1, 127.0, 127.0, 126.1, 122.8, 122.5, 122.4. HRMS (ESI⁺) (MeOH) [M - NO₃]⁺: *m/z* calcd for C₁₃H₁₄ClN₆Pt: 484.0616, found: 484.0627.

ASSOCIATED CONTENT

(Word Style “TE_Supporting_Information”). **Supporting Information.** A brief statement in nonsentence format listing the contents of material supplied as Supporting Information should be included, ending with “This material is available free of charge via the Internet at <http://pubs.acs.org>.” For instructions on what should be included in the Supporting Information as well as how to prepare this material for publication, refer to the journal’s Instructions for Authors.

AUTHOR INFORMATION

Corresponding Author

Darren Griffith, email: dgriffith@rcsi.com

Author Contributions

The manuscript was written through contributions of all authors. All authors have given approval to the final version of the manuscript. ‡These authors contributed equally.

Funding Sources

Any funds used to support the research of the manuscript should be placed here (per journal style).

ACKNOWLEDGMENT

DMG, POD and FOS gratefully acknowledge funding received from the Synthesis and Solid State Pharmaceutical Centre (SSPC), financed by a research grant from Science Foundation Ireland (SFI) and co-funded under the European Regional Development Fund under [grant number 12/RC/2275_P2]. This work was supported by the National Science Foundation [CHE2109255 to V. J. D., NSF DGE-2022168 to ASG and KRA]. This work is also supported by the Department of Chemistry and Biochemistry and the Material Science Institute at the University of Oregon.

REFERENCES

1. Forgie, B. N.; Prakash, R.; Telleria, C. M., Revisiting the Anti-Cancer Toxicity of Clinically Approved Platinating Derivatives. *Int. J. Mol. Sci.* **2022**, *23* (23).
2. Rottenberg, S.; Disler, C.; Perego, P., The rediscovery of platinum-based cancer therapy. *Nat. Rev. Cancer* **2021**, *21* (1), 37-50.
3. O'Dowd, P. D.; Sutcliffe, D. F.; Griffith, D. M., Oxaliplatin and its derivatives – An overview. *Coord. Chem. Rev.* **2023**, *497*, 215439.
4. Fanelli, M.; Formica, M.; Fusi, V.; Giorgi, L.; Micheloni, M.; Paoli, P., New trends in platinum and palladium complexes as antineoplastic agents. *Coord. Chem. Rev.* **2016**, *310*, 41-79.
5. Park, G. Y.; Wilson, J. J.; Song, Y.; Lippard, S. J., Phenanthriplatin, a monofunctional DNA-binding platinum anticancer drug candidate with unusual potency and cellular activity profile. *PNAS* **2012**, *109* (30), 11987-92.
6. Zhou, W.; Almeqdadi, M.; Xifaras, M. E.; Riddell, I. A.; Yilmaz Ö. H.; Lippard, S. J., The effect of geometric isomerism on the anticancer activity of the monofunctional platinum complex trans-[Pt(NH₃)(2)(phenanthridine)Cl]NO₃. *ChemComm* **2018**, *54* (22), 2788-2791.
7. Veciani, D.; Melchior, A.; Tolazzi, M.; Cerón-Carrasco, J. P., Using Theory To Reinterpret the Kinetics of Monofunctional Platinum Anticancer Drugs: Stacking Matters. *J. Am. Chem. Soc.* **2018**, *140* (43), 14024-14027.
8. Almaqwashi, A. A.; Zhou, W.; Naufer, M. N.; Riddell, I. A.; Yilmaz, Ö. H.; Lippard, S. J.; Williams, M. C., DNA Intercalation Facilitates Efficient DNA-Targeted Covalent Binding of Phenanthriplatin. *J. Am. Chem. Soc.* **2019**, *141* (4), 1537-1545.
9. Dabbish, E.; Russo, N.; Sicilia, E., Rationalization of the Superior Anticancer Activity of Phenanthriplatin: An In-Depth Computational Exploration. *Chem. Eur. J.* **2020**, *26* (1), 259-268.
10. Veciani, D.; Tolazzi, M.; Cerón-Carrasco, J. P.; Melchior, A., Intercalation Ability of Novel Monofunctional Platinum Anticancer Drugs: A Key Step in Their Biological Action. *J. Chem. Inf. Model.* **2021**, *61* (9), 4391-4399.
11. Kellinger, M. W.; Park, G. Y.; Chong, J.; Lippard, S. J.; Wang, D., Effect of a Monofunctional Phenanthriplatin-DNA Adduct on RNA Polymerase II Transcriptional Fidelity and Translesion Synthesis. *J. Am. Chem. Soc.* **2013**, *135* (35), 13054-13061.
12. Gregory, M. T.; Park, G. Y.; Johnstone, T. C.; Lee, Y. S.; Yang, W.; Lippard, S. J., Structural and mechanistic studies of polymerase η bypass of phenanthriplatin DNA damage. *PNAS* **2014**, *111* (25), 9133-8.
13. Riddell, I. A.; Agama, K.; Park, G. Y.; Pommier, Y.; Lippard, S. J., Phenanthriplatin Acts As a Covalent Poison of Topoisomerase II Cleavage Complexes. *ACS Chem. Biol.* **2016**, *11* (11), 2996-3001.
14. Urankar, D.; Košmrlj, J., Preparation of diazenecarboxamide-carboplatin conjugates by click chemistry. *Inorganica Chim. Acta* **2010**, *363* (14), 3817-3822.
15. Wirth, R.; White, J. D.; Moghaddam, A. D.; Ginzburg, A. L.; Zakharov, L. N.; Haley, M. M.; DeRose, V. J., Azide vs Alkyne Functionalization in Pt(II) Complexes for Post-treatment Click Modification: Solid-State Structure, Fluorescent Labeling, and Cellular Fate. *J. Am. Chem. Soc.* **2015**, *137* (48), 15169-15175.
16. Guerrero, A. S.; O'Dowd, P. D.; Pigg, H. C.; Alley, K. R.; Griffith, D. M.; DeRose, V. J., Comparison of click-capable oxaliplatin and cisplatin derivatives to better understand Pt(ii)-induced nucleolar stress. *RSC Chem. Biol.* **2023**.
17. Bruno, P. M.; Liu, Y.; Park, G. Y.; Murai, J.; Koch, C. E.; Eisen, T. J.; Pritchard, J. R.; Pommier, Y.; Lippard, S. J.; Hemann, M. T., A subset of platinum-containing chemotherapeutic agents kills cells by inducing ribosome biogenesis stress. *Nat. Med.* **2017**, *23* (4), 461-471.
18. Yang, K.; Yang, J.; Yi, J., Nucleolar Stress: hallmarks, sensing mechanism and diseases. *Cell Stress* **2018**, *2* (6), 125-140.
19. Ozdian, T.; Holub, D.; Maceckova, Z.; Varanasi, L.; Rylova, G.; Rehulka, J.; Vaclavkova, J.; Slavik, H.; Moudry, P.; Znojek, P.; Stankova, J.; de Sanctis, J. B.; Hajduch, M.; Dzubak, P., Proteomic profiling reveals DNA damage, nucleolar and ribosomal stress are the main responses to oxaliplatin treatment in cancer cells. *J. Proteomics* **2017**, *162*, 73-85.
20. Sutton, E. C.; McDevitt, C. E.; Prochnau, J. Y.; Yglesias, M. V.; Mroz, A. M.; Yang, M. C.; Cunningham, R. M.; Hendon, C. H.; DeRose, V. J., Nucleolar Stress Induction by Oxaliplatin and Derivatives. *J. Am. Chem. Soc.* **2019**, *141* (46), 18411-18415.
21. Sutton, E. C.; DeRose, V. J., Early nucleolar responses differentiate mechanisms of cell death induced by oxaliplatin and cisplatin. *J. Biol. Chem.* **2021**, *296*, 100633.
22. McDevitt, C. E.; Guerrero, A. S.; Smith, H. M.; DeRose, V. J., Influence of Ring Modifications on Nucleolar Stress Caused by Oxaliplatin-Like Compounds**. *ChemBioChem* **2022**, *23* (14), e202200130.
23. Pigg, H. C.; Yglesias, M. V.; Sutton, E. C.; McDevitt, C. E.; Shaw, M.; DeRose, V. J., Time-Dependent Studies of Oxaliplatin and Other Nucleolar Stress-Inducing Pt(II) Derivatives. *ACS Chem. Biol.* **2022**, *17* (8), 2262-2271.
24. Schmidt, H. B.; Jaafar, Z. A.; Wulff, B. E.; Rodencal, J. J.; Hong, K.; Aziz-Zanjani, M. O.; Jackson, P. K.; Leonetti, M. D.; Dixon, S. J.; Rohatgi, R.; Brandman, O., Oxaliplatin disrupts nucleolar function through biophysical disintegration. *Cell Rep.* **2022**, *41* (6), 111629.
25. Nechay, M.; Wang, D.; Kleiner, R. E., Inhibition of nucleolar transcription by oxaliplatin involves ATM/ATR kinase signaling. *Cell Chem. Biol.* **2023**, *30* (8), 906-919.e4.

26. McDevitt, C. E.; Yglesias, M. V.; Mroz, A. M.; Sutton, E. C.; Yang, M. C.; Hendon, C. H.; DeRose, V. J., Monofunctional platinum(II) compounds and nucleolar stress: is phenanthriplatin unique? *J. Biol. Inorg. Chem.* **2019**, *24* (6), 899-908.
27. Mitchell, R. J.; Kriger, S. M.; Fenton, A. D.; Havrylyuk, D.; Pandeya, A.; Sun, Y.; Smith, T.; DeRouchey, J. E.; Unrine, J. M.; Oza, V.; Blackburn, J. S.; Wei, Y.; Heidary, D. K.; Glazer, E. C., A monoadduct generating Ru(II) complex induces ribosome biogenesis stress and is a molecular mimic of phenanthriplatin. *RSC Chem. Biol.* **2023**, *4* (5), 344-353.
28. Farrer, N. J.; Griffith, D. M., Exploiting azide-alkyne click chemistry in the synthesis, tracking and targeting of platinum anticancer complexes. *Curr. Opin. Chem. Biol.* **2020**, *55*, 59-68.
29. Sutton, E. C.; McDevitt, C. E.; Yglesias, M. V.; Cunningham, R. M.; DeRose, V. J., Tracking the cellular targets of platinum anticancer drugs: Current tools and emergent methods. *Inorganica Chim. Acta* **2019**, *498*, 118984.
30. Cunningham, R. M.; DeRose, V. J., Platinum Binds Proteins in the Endoplasmic Reticulum of *S. cerevisiae* and Induces Endoplasmic Reticulum Stress. *ACS Chem. Biol.* **2017**, *12* (11), 2737-2745.
31. Osborn, M. F.; White, J. D.; Haley, M. M.; DeRose, V. J., Platinum-RNA Modifications Following Drug Treatment in *S. cerevisiae* Identified by Click Chemistry and Enzymatic Mapping. *ACS Chem. Biol.* **2014**, *9* (10), 2404-2411.
32. Moghaddam, A. D.; White, J. D.; Cunningham, R. M.; Loes, A. N.; Haley, M. M.; DeRose, V. J., Convenient detection of metal-DNA, metal-RNA, and metal-protein adducts with a click-modified Pt(II) complex. *Dalton Trans.* **2015**, *44* (8), 3536-3539.
33. White, J. D.; Guzman, L. E.; Zakharov, L. N.; Haley, M. M.; DeRose, V. J., An Alkyne-Appended, Click-Ready Pt(II) Complex with an Unusual Arrangement in the Solid State. *Angew. Chem. Int. Ed.* **2015**, *54* (3), 1032-1035.
34. Moretton, A.; Slysikova, J.; Simaan, M. E.; Arasa-Verge, E. A.; Meyenberg, M.; Cerrón-Infantes, D. A.; Unterlass, M. M.; Loizou, J. I., Clickable Cisplatin Derivatives as Versatile Tools to Probe the DNA Damage Response to Chemotherapy. *Front. Oncol.* **2022**, *12*, 874201.
35. Johnstone, T. C.; Lippard, S. J., The Chiral Potential of Phenanthriplatin and Its Influence on Guanine Binding. *J. Am. Chem. Soc.* **2014**, *136* (5), 2126-2134.
36. van Sluis, M.; McStay, B., Nucleolar reorganization in response to rDNA damage. *Curr. Opin. Cell Biol.* **2017**, *46*, 81-86.
37. Koike, A.; Nishikawa, H.; Wu, W.; Okada, Y.; Venkitaraman, A. R.; Ohta, T., Recruitment of Phosphorylated NPM1 to Sites of DNA Damage through RNF8-Dependent Ubiquitin Conjugates. *Cancer Res.* **2010**, *70* (17), 6746-6756.
38. Eeftens, J. M.; van der Torre, J.; Burnham, D. R.; Dekker, C., Copper-free click chemistry for attachment of biomolecules in magnetic tweezers. *BMC Biophys.* **2015**, *8* (1), 9.
39. Schindelin, J.; Arganda-Carreras, I.; Frise, E.; Kaynig, V.; Longair, M.; Pietzsch, T.; Preibisch, S.; Rueden, C.; Saalfeld, S.; Schmid, B.; Tinevez, J.-Y.; White, D. J.; Hartenstein, V.; Eliceiri, K.; Tomancak, P.; Cardona, A., Fiji: an open-source platform for biological-image analysis. *Nat. Methods* **2012**, *9* (7), 676-682.
40. Rueden, C. T.; Schindelin, J.; Hiner, M. C.; DeZonia, B. E.; Walter, A. E.; Arena, E. T.; Eliceiri, K. W., ImageJ2: ImageJ for the next generation of scientific image data. *BMC Bioinform.* **2017**, *18* (1), 529.
41. van der Walt, S.; Schönberger, J. L.; Nunez-Iglesias, J.; Boulogne, F.; Warner, J. D.; Yager, N.; Guillaert, E.; Yu, T., scikit-image: image processing in Python. *PeerJ* **2014**, *2*, e453.
42. Carpenter, A. E.; Jones, T. R.; Lamprecht, M. R.; Clarke, C.; Kang, I. H.; Friman, O.; Guertin, D. A.; Chang, J. H.; Lindquist, R. A.; Moffat, J.; Golland, P.; Sabatini, D. M., CellProfiler: image analysis software for identifying and quantifying cell phenotypes. *Genome Biol.* **2006**, *7* (10), R100.

Click-Capable Phenanthriplatin Derivatives as Tools to Study Pt(II)-Induced Nucleolar Stress

Paul D. O'Dowd,^{a,b} Andres S. Guerrero,^c Hannah C. Pigg,^c Katelyn R. Alley,^c Fiona O'Neill,^d Justine Meiller,^d Chloe Hobbs,^a Daniel A. Rodrigues,^a Brendan Twamley,^e Finbarr O'Sullivan,^d Victoria J. DeRose,^c Darren M. Griffith*^{a,b}.

^a Department of Chemistry, Royal College of Surgeons in Ireland, Dublin, Ireland

^b SSPC, the Science Foundation Ireland Research Centre for Pharmaceuticals

^c Department of Chemistry and Biochemistry, University of Oregon, Eugene, OR, USA

^d Life Science Institute, Dublin City University, Dublin, Ireland.

^e Department of Chemistry, Trinity College Dublin, Dublin, Ireland.

Contents

NPM1 Average Coefficient of Variation for 1,2 and 3:	15
In-vitro activity of 3 and Pt controls:	15
Synthesis & Characterization of Ligands:	17
SI NMR (¹H & ¹³C) and HRMS Spectra for 1, 2 and 3:	21
Single crystal X-Ray diffraction:	26

NPM1 Average Coefficient of Variation for 1,2 and 3:

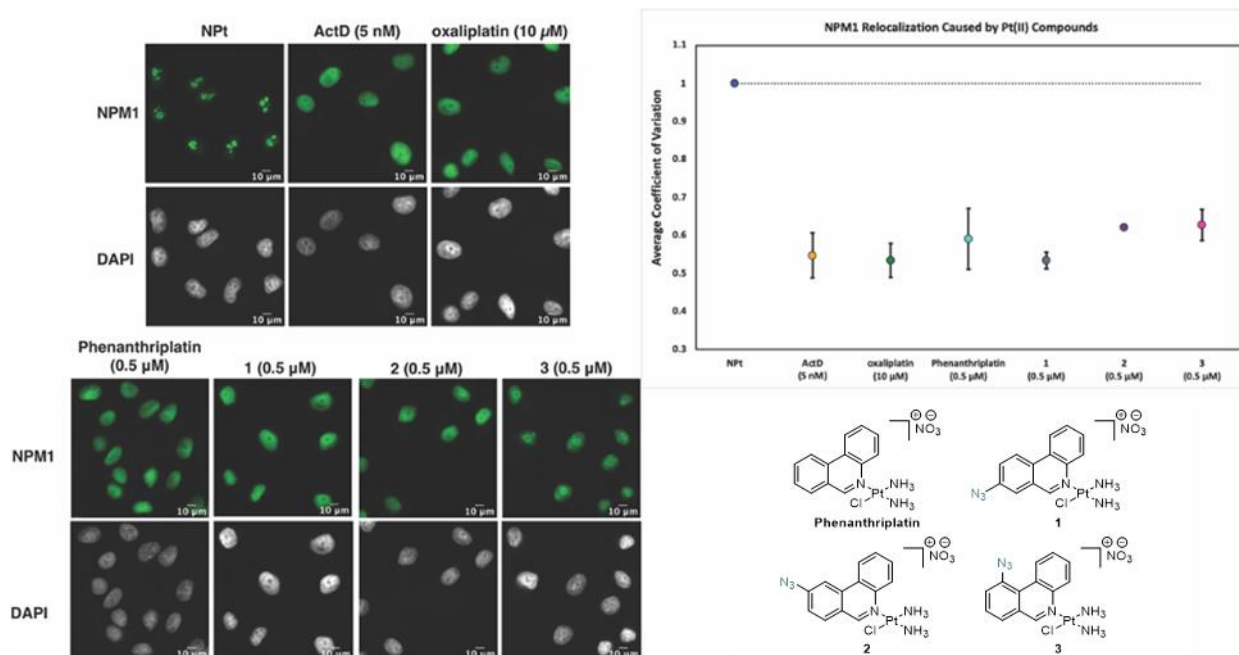


Figure S1. Average Coefficient of Variation (CV) quantification of NPM1 relocalization induced by **1**, **2** and **3** along with representative cell images of each treatment. Treatment conditions indicated (either 10 μM or 0.5 μM for Pt complexes, 5 nM for ActD) in A549 cells at 24 hr treatment; CV calculations, and boxplot presentations as described in the Experimental Section. For each treatment data set, average of CV of 3 trials along with std.

In-vitro activity of **3** and Pt controls:

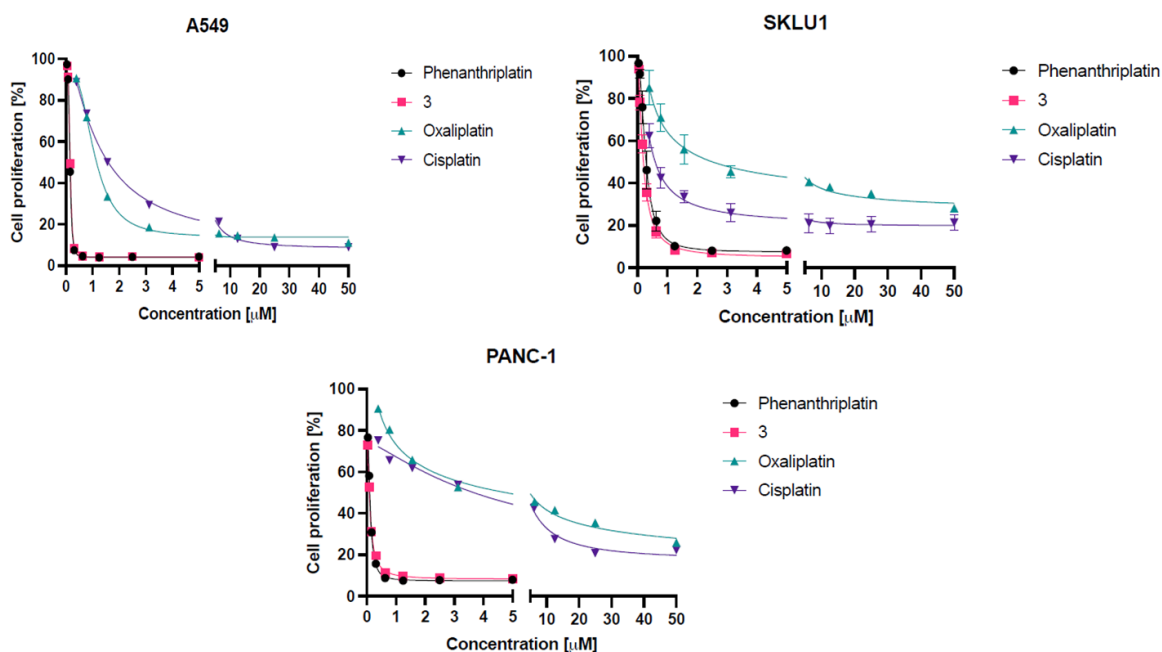
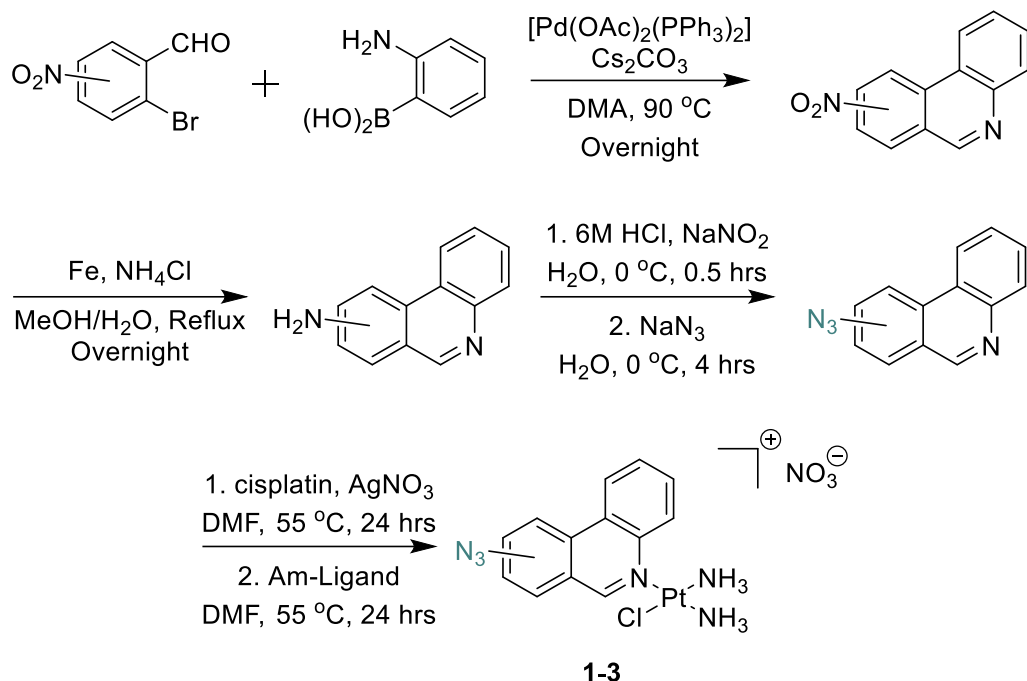


Figure S2. *In-vitro* proliferation of A549, SK-LU-1 and PANC-1 cells following treatment with **3** and Pt-controls for 6 days.

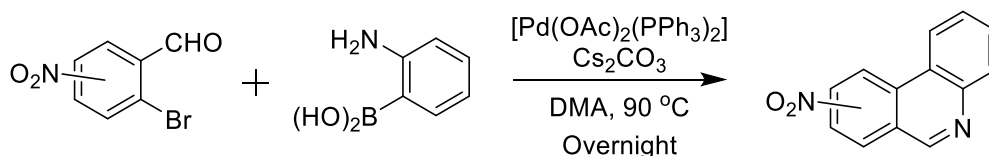
Synthesis & Characterization of Ligands:

**Note: While no issues were encountered during our handling of the organic azides and 1, 2 and 3, organic and inorganic azides are known to be neurotoxic and explosive in nature. As such, care should be taken if preparing the compounds described below.*

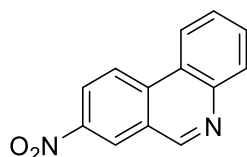
Complete synthetic route for the synthesis of complexes 1-3:



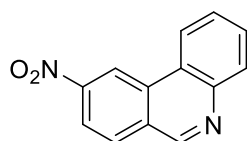
General Suzuki Coupling Procedure:



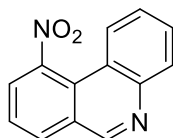
2-bromo-*n*-nitrobenzaldehyde (1.50 g, 6.52 mmol), (2-aminophenyl)boronic acid (1.07 g, 7.83 mmol) and cesium carbonate (3.19 g, 9.78 mmol) were dissolved in DMA (10 mL). To this was added a mixture of $[\text{Pd}(\text{OAc})_2]$ (73.2 mg, 0.33 mmol) and triphenylphosphine (427.6 mg, 1.63 mmol) in DMA (5 mL). The resulting mixture was heated to 90°C and stirred under Ar for 2 days. After stirring, the reaction mixture was cooled to room temperature and diluted with water (50 mL). The product was then extracted with ethyl acetate (3 x 50 mL), washed with brine (3 x 50 mL) and dried over anhydrous sodium sulphate. The solvent was removed under reduced pressure to and the product purified by column chromatography (70: 30 petroleum ether: ethyl acetate).



8-nitrophenanthridine was isolated as a brown solid, (693 mg, 47%). ^1H NMR (400 MHz, CDCl_3) δ 9.39 (s, 1H), 8.94 (d, 1H, $J = 2.2$ Hz), 8.73 (d, 1H, $J = 9.1$ Hz), 8.65 – 8.57 (m, 2H), 8.28 – 8.22 (m, 1H), 7.91 – 7.84 (m, 1H), 7.82 – 7.74 (m, 1H). ^{13}C NMR (101 MHz, CDCl_3) δ 153.28, 146.47, 145.78, 136.53, 130.99, 130.76, 128.31, 125.67, 124.75, 124.65, 123.89, 123.14, 122.94. MS (ESI+) $[\text{M}+\text{H}]^+$: m/z calcd for $\text{C}_{13}\text{H}_9\text{N}_2\text{O}_2$: 225.1, found: 224.8.

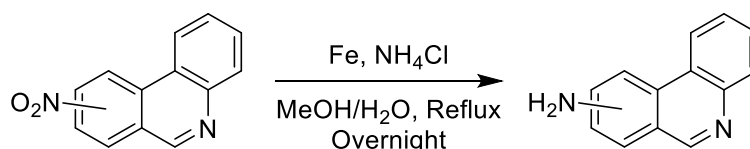


9-nitrophenanthridine was isolated as a brown solid, (392 mg, 27%). ^1H NMR (400 MHz, CDCl_3) δ 9.49 (d, 1H, $J = 1.4$ Hz), 9.39 (s, 1H), 8.64 (d, 1H, $J = 8.1$ Hz), 8.49 (dd, 1H, $J = 8.7, 2.0$ Hz), 8.26 (d, 1H, $J = 8.0$ Hz), 8.22 (d, 1H, $J = 8.7$ Hz), 7.86 (m, 1H), 7.81 (m, 1H). ^{13}C NMR (101 MHz, CDCl_3) δ 152.44, 148.96, 145.03, 132.87, 130.82, 130.48, 130.34, 128.74, 128.52, 123.67, 122.57, 121.48, 118.44. (ESI+) $[\text{M}+\text{H}]^+$: m/z calcd for $\text{C}_{13}\text{H}_9\text{N}_2\text{O}_2$: 225.1, found: 224.7.



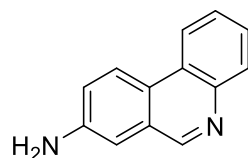
10-nitrophenanthridine was isolated as a red solid, (964 mg, 66%). ^1H NMR (400 MHz, CDCl_3) δ 9.31 (s, 1H), 8.27 – 8.19 (m, 2H), 8.09 (dd, 1H, $J = 8.5, 0.7$ Hz), 7.95 (dd, 1H, $J = 7.6, 1.2$ Hz), 7.85 – 7.73 (m, 2H), 7.64 (m, 1H). ^{13}C NMR (101 MHz, CDCl_3) δ 152.45, 147.74, 145.71, 132.34, 131.04, 130.36, 128.09, 127.73, 127.04, 126.15, 124.15, 123.53, 119.64. (ESI+) $[\text{M}+\text{H}]^+$: m/z calcd for $\text{C}_{13}\text{H}_9\text{N}_2\text{O}_2$: 225.1, found: 225.1.

General Procedure for Reduction of Nitro-group:

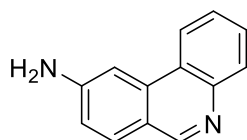


n-nitrophenanthridine (1.00 g, 4.46 mmol), iron powder (1.99 g, 35.68 mmol), and ammonium chloride (2.39 g, 44.60 mol) were added to a round bottom flask. Methanol (40 mL) and water (5 mL) were added to the mixture and the resulting suspension heated to 75 °C. The mixture was stirred under reflux overnight and reaction completion was confirmed by TLC the following day. The reaction mixture was allowed to cool to room temperature and the pH of the solution was adjusted to < 5 using HCl (1 M). The solution was extracted with ethyl acetate (2 x 25 mL) and the combined organic layers discarded. The pH of the aqueous phase was then

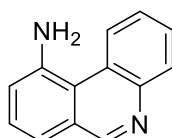
adjusted to > 10 using NaOH (1 M) and the phase again extracted with ethyl acetate (3 x 50 mL). The organic layers were then combined, washed with brine (2 x 25 mL) and dried over anhydrous sodium sulphate. The solvent was removed under reduced pressure to give a crude solid which was purified by column chromatography (70: 30 ethyl acetate: petroleum ether).



Phenanthridin-8-amine was isolated as a brown solid, (693 mg, 80%). ^1H NMR (400 MHz, CDCl_3) δ 9.08 (s, 1H), 8.44 – 8.37 (m, 2H), 8.13 – 8.07 (m, 1H), 7.65 – 7.57 (m, 2H), 7.26 – 7.22 (m, 1H), 7.17 (d, 1H, $J = 2.3$ Hz), 4.11 (s, 2H). ^{13}C NMR (101 MHz, CDCl_3) δ 152.87, 146.05, 143.35, 130.13, 128.18, 127.17, 127.13, 125.34, 124.75, 123.46, 121.49, 121.28, 110.59. (ESI+) $[\text{M}+\text{H}]^+$: m/z calcd for $\text{C}_{13}\text{H}_{11}\text{N}_2$: 195.1, found: 194.9.

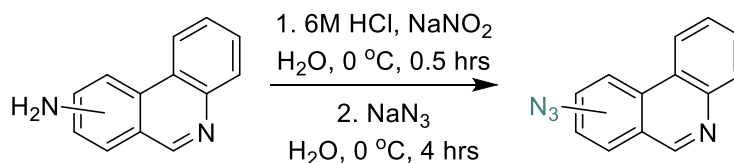


Phenanthridin-9-amine was isolated as a brown solid, (788 mg, 91%). ^1H NMR (400 MHz, CDCl_3) δ 9.06 (s, 1H), 8.41 (d, 1H, $J = 8.1$ Hz), 8.10 (d, 1H, $J = 8.2$ Hz), 7.83 (d, 1H, $J = 8.5$ Hz), 7.72 – 7.66 (m, 2H), 7.60 (m, 1H), 7.04 (m, 1H), 4.29 (s, 2H). ^{13}C NMR (101 MHz, CDCl_3) δ 152.97, 149.32, 145.05, 134.87, 130.76, 130.00, 128.67, 126.26, 123.79, 122.37, 120.30, 117.31, 103.80. (ESI+) $[\text{M}+\text{H}]^+$: m/z calcd for $\text{C}_{13}\text{H}_{11}\text{N}_2$: 195.1, found: 194.8.

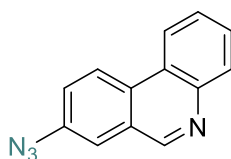


Phenanthridin-10-amine was isolated as a brown solid, (768 mg, 89%). ^1H NMR (400 MHz, CDCl_3) δ 9.16 (s, 1H), 9.05 (dd, $J = 8.3, 1.0$ Hz, 1H), 8.20 (dd, $J = 8.0, 1.3$ Hz, 1H), 7.73 – 7.67 (m, 1H), 7.67 – 7.61 (m, 1H), 7.55 – 7.49 (m, 2H), 7.18 (dd, $J = 6.2, 2.6$ Hz, 1H). ^{13}C NMR (101 MHz, CDCl_3) δ 154.51, 145.07, 144.61, 130.45, 128.71, 127.87, 127.64, 126.79, 124.97, 121.34, 120.58, 119.42. (ESI+) $[\text{M}+\text{H}]^+$: m/z calcd for $\text{C}_{13}\text{H}_{11}\text{N}_2$: 195.1, found: 195.1.

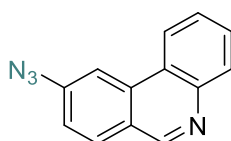
General Procedure for Nitro to Azide Transformation:



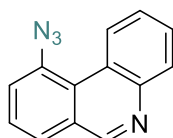
6M HCl (3.9 mL, 23.4 mmol) was added to phenanthridin-*n*-amine (0.75g, 3.86 mmol) and the resulting mixture cooled to 0 °C in an ice bath. Sodium nitrite (0.525 g, 7.623 mmol) in water (5 mL) was added dropwise to this mixture with vigorous stirring, and the resulting solution stirred for 30 minutes at 0 °C. Following this a solution of sodium azide (0.99 g, 15.24 mmol) in water (5 mL) was added dropwise and the reaction mixture stirred for a further 4 hour at 0 °C. Following reaction completion, the pH of the solution was adjusted to > 7 with sodium hydroxide (1 M) and the product extracted with ethyl acetate (3 x 50 mL). The organic layers were combined, washed with brine (2 x 25 mL) and dried over anhydrous sodium sulphate. The solvent was removed under reduced pressure and the crude product purified by column chromatography (50: 50 petroleum ether: ethyl acetate).



8-azidophenanthridine was isolated as a white solid, (544 mg, 64%). ¹H NMR (400 MHz, DMSO) δ 9.48 (s, 1H), 8.88 (d, 1H, *J* = 8.9 Hz), 8.84 – 8.77 (m, 1H), 8.20 – 8.13 (m, 1H), 8.06 (d, 1H, *J* = 2.3 Hz), 7.81 (m, 2H), 7.72 (dd, 1H, *J* = 8.8, 2.4 Hz). ¹³C NMR (101 MHz, DMSO) δ 152.13, 141.36, 139.52, 129.45, 129.20, 128.15, 128.03, 126.55, 124.76, 124.58, 123.61, 123.02, 118.04. (ESI+) [M-N₂]⁺: *m/z* calcd for C₁₃H₈N₂: 192.1, found: 192.6.



9-azidophenanthridine was isolated as a white solid, (485 mg, 57%). ¹H NMR (400 MHz, CDCl₃) δ 9.21 (s, 1H), 8.48 (d, 1H, *J* = 8.0 Hz), 8.18 (d, 1H, *J* = 8.0 Hz), 8.13 (d, 1H, *J* = 1.6 Hz), 8.03 (d, 1H, *J* = 8.5 Hz), 7.81 – 7.73 (m, 1H), 7.73 – 7.64 (m, 1H), 7.36 (dd, 1H, *J* = 8.5, 2.1 Hz). ¹³C NMR (101 MHz, CDCl₃) δ 152.82, 144.94, 143.02, 134.12, 130.93, 130.38, 129.45, 127.30, 123.87, 123.39, 122.38, 119.53, 111.06. (ESI+) [M-N₂]⁺: *m/z* calcd for C₁₃H₈N₂: 192.1, found: 192.3.



10-azidophenanthridine was isolated as a white solid, (655 mg, 77%). ¹H NMR (400 MHz, CDCl₃) δ 9.65 (dd, 1H, *J* = 8.4, 1.0 Hz), 9.21 (s, 1H), 8.19 (dd, 1H, *J* = 8.1, 1.2 Hz), 7.84 (dd, 1H, *J* = 7.6, 1.1 Hz), 7.79 – 7.63 (m, 4H). ¹³C NMR (101 MHz, CDCl₃) δ 153.47, 145.35, 137.06, 130.28, 128.81, 128.68, 127.58, 127.39, 127.12, 126.01, 124.36, 123.32, 121.31. (ESI+) [M-N₂]⁺: *m/z* calcd for C₁₃H₈N₂: 192.1, found: 193.1.

SI NMR (^1H & ^{13}C) and HRMS Spectra for 1, 2 and 3:

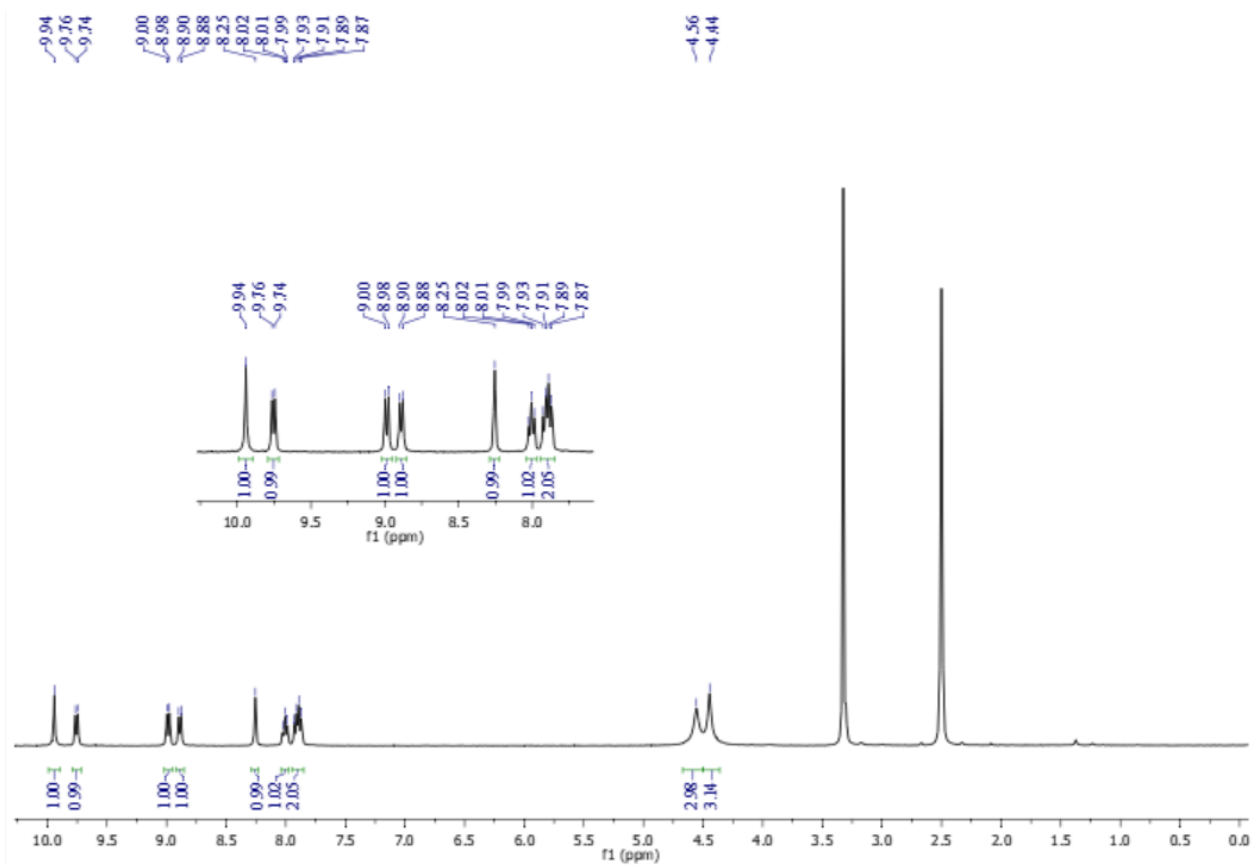


Figure S3. ^1H NMR of 1 in DMSO-d_6

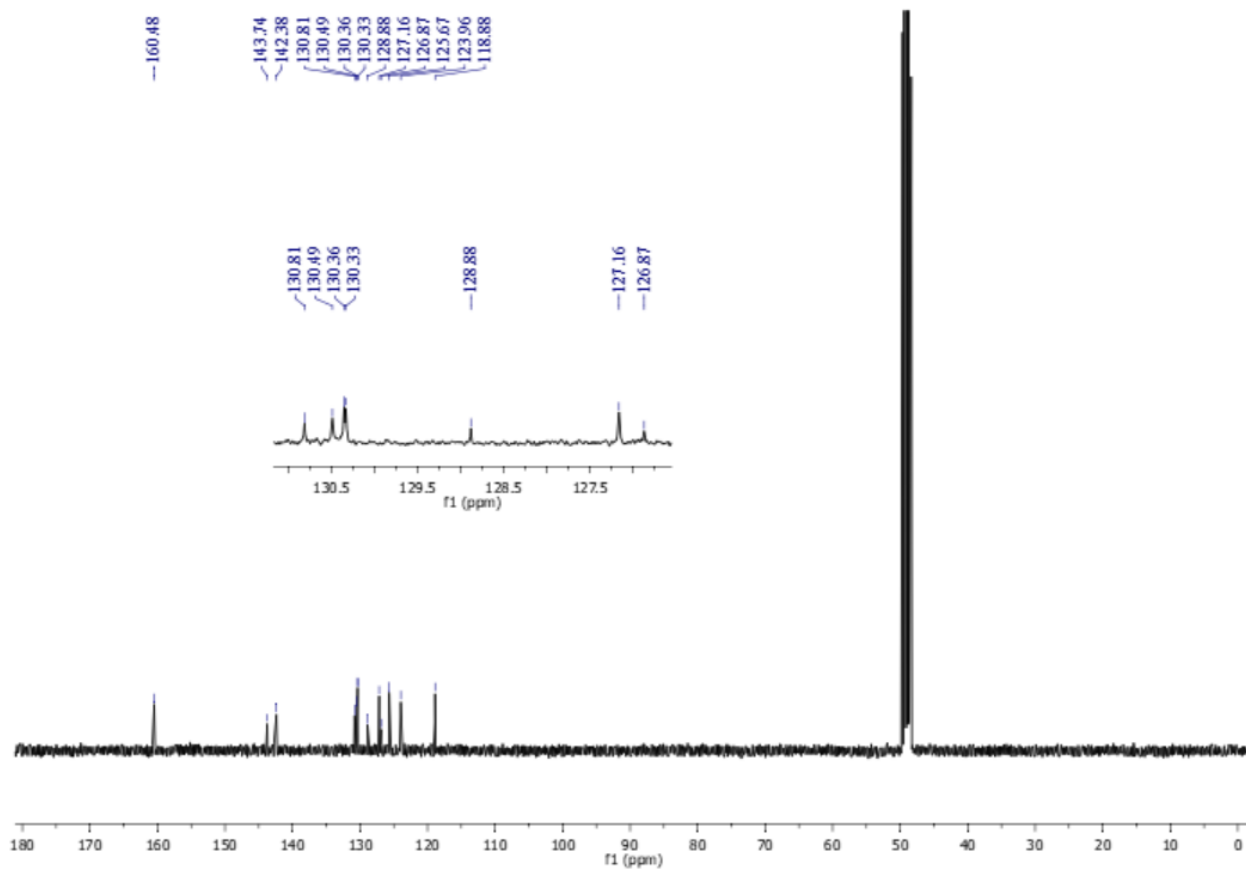


Figure S4. ^{13}C NMR of **1** in MeOD- d_4

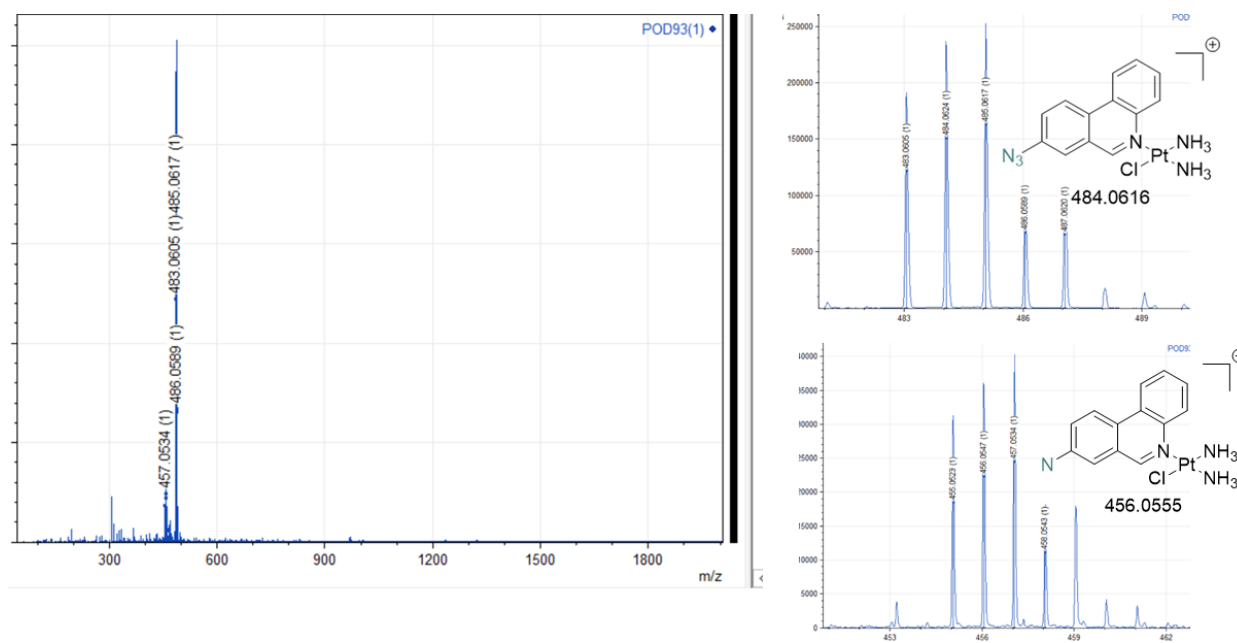


Figure S5. HRMS (ESI+) of **1**

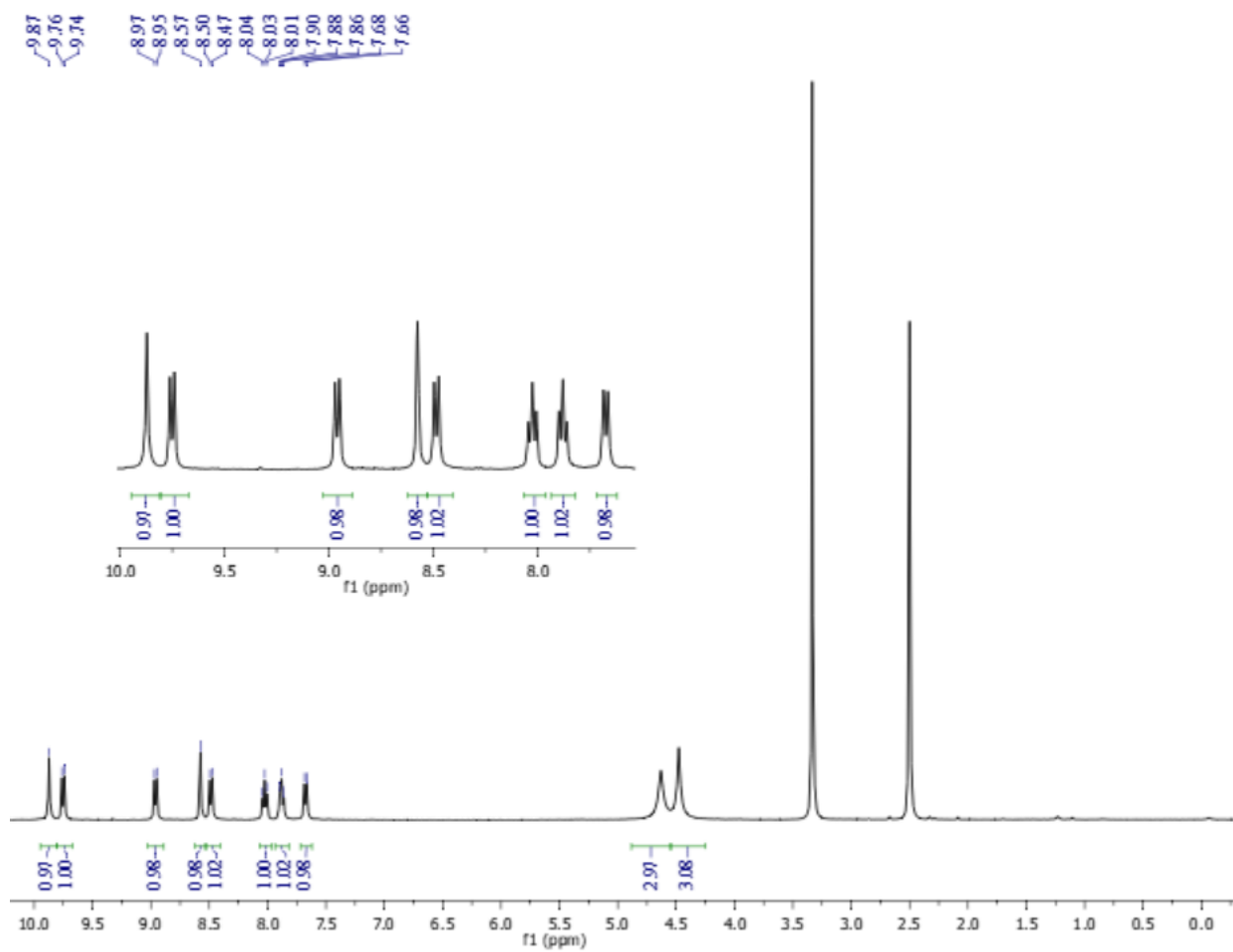


Figure S6. ^1H NMR of **2** in DMSO-d_6

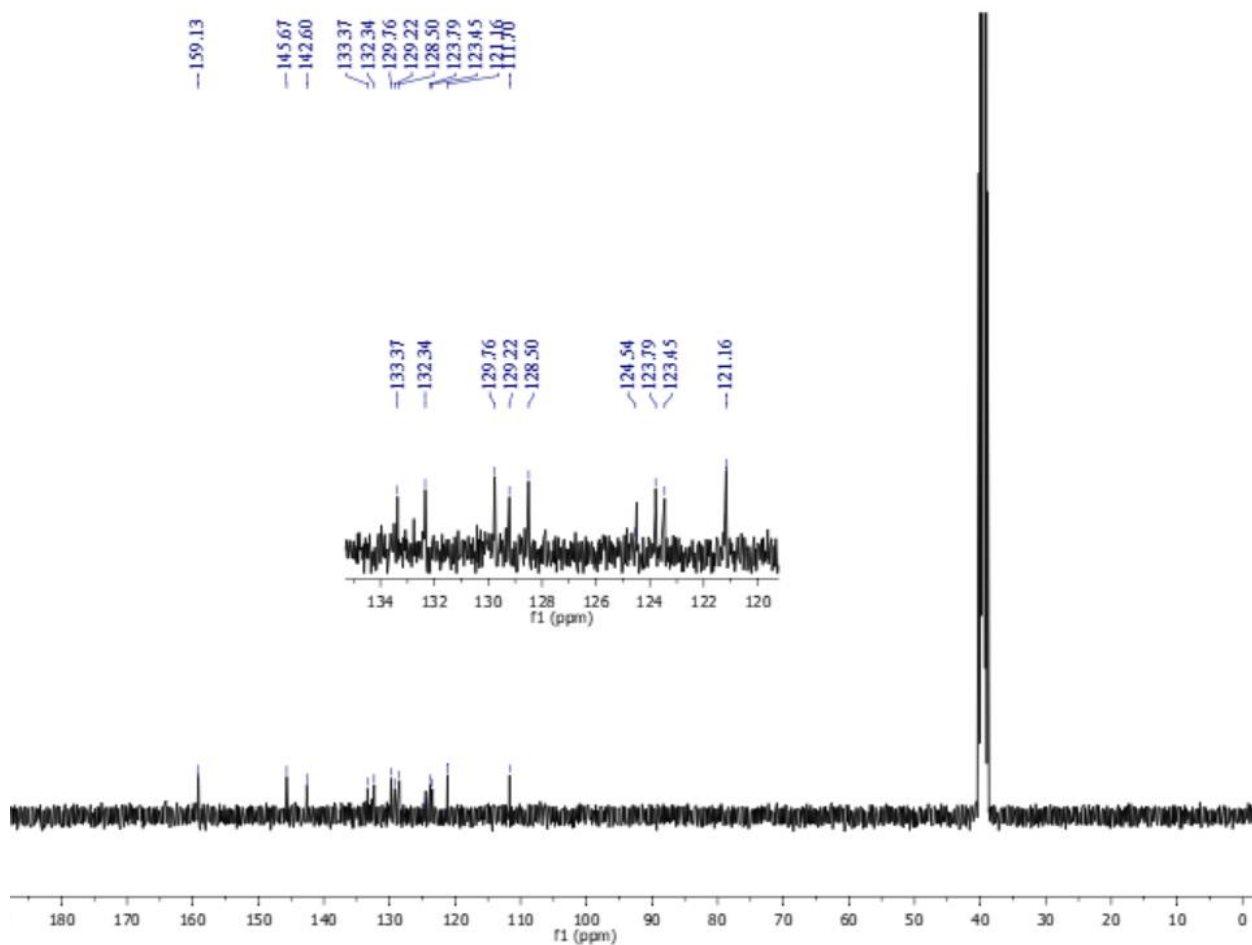


Figure S7. ^{13}C NMR of **2** in DMSO-d_6

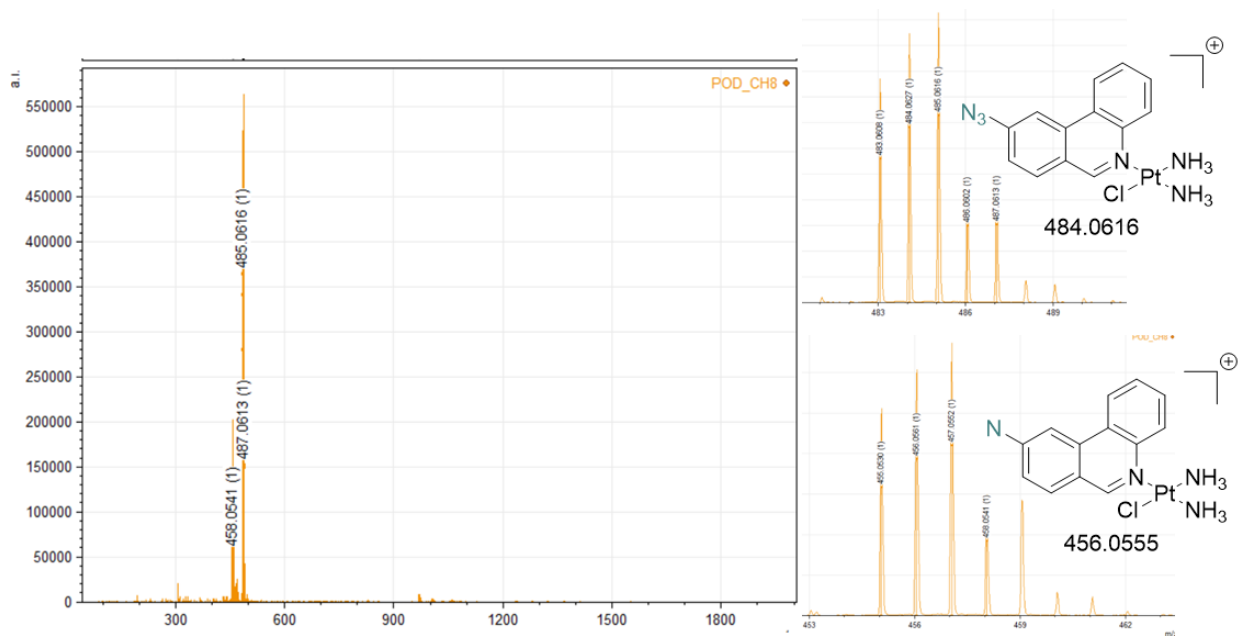


Figure S8. HRMS (ESI+) of **2**

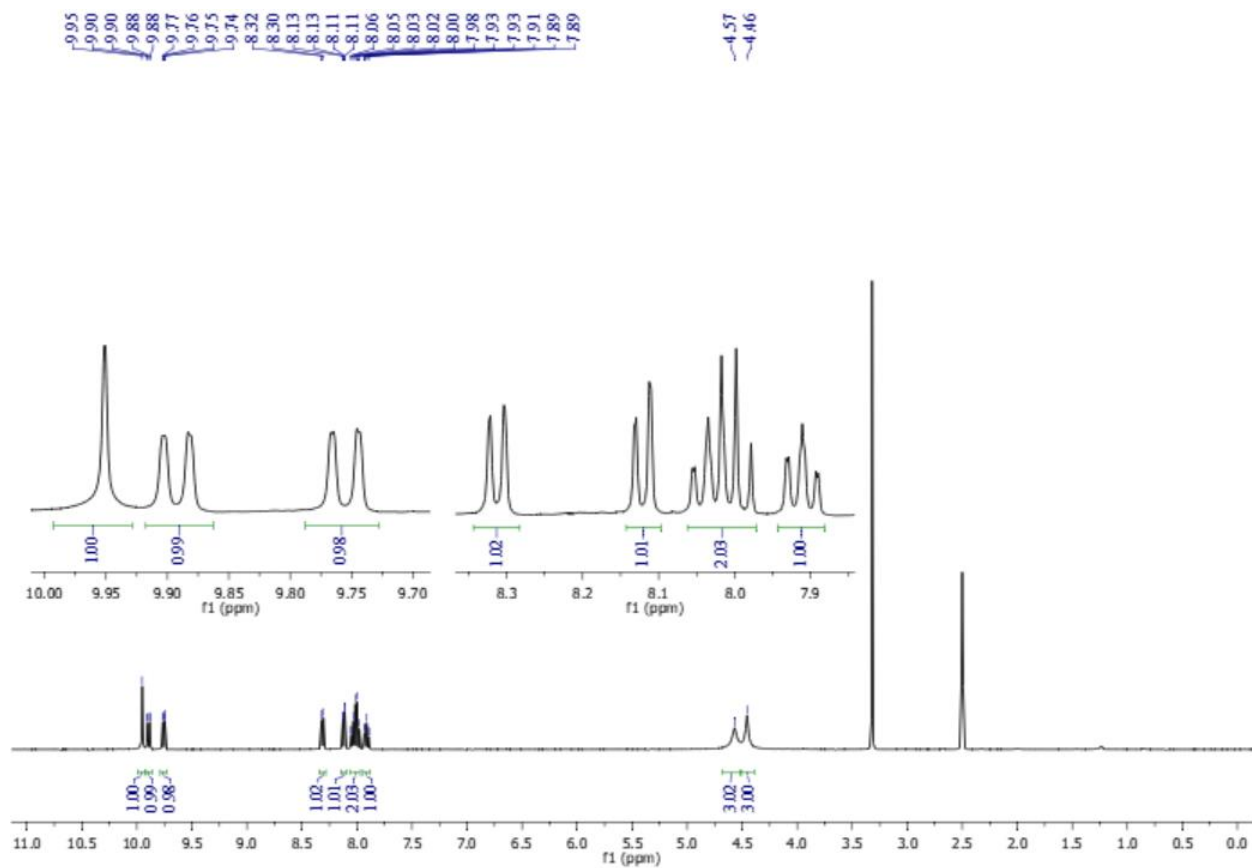


Figure S9. ^1H NMR of **3** in DMSO-d_6

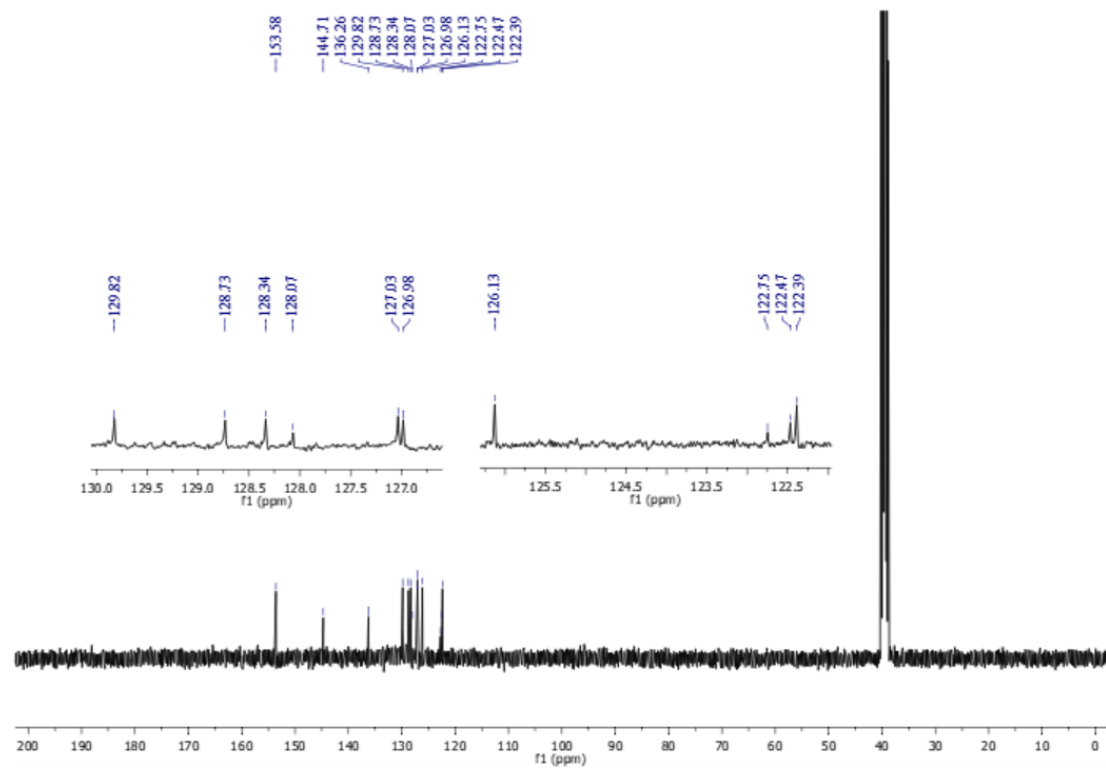


Figure S10. ^{13}C NMR of **3** in DMSO-d_6

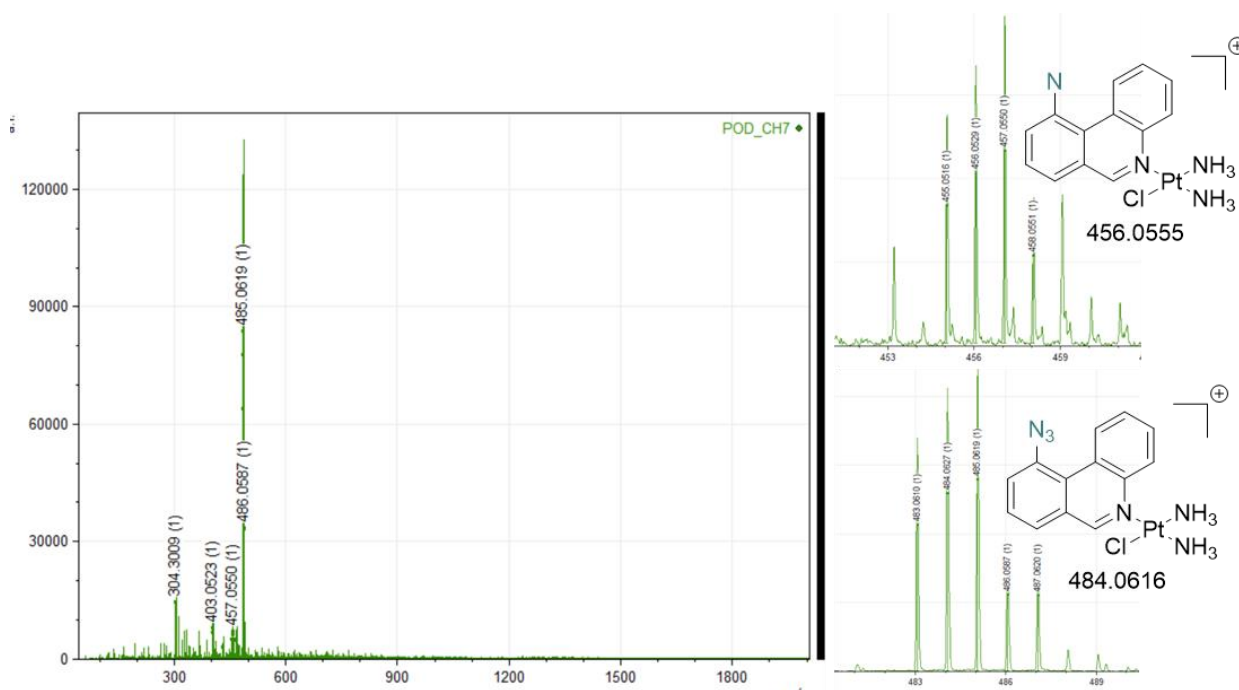


Figure S11. HRMS (ESI+) of **3**

Single crystal X-Ray diffraction:

The X-ray intensity data for **1** were measured ($\lambda = 1.54178 \text{ \AA}$) on a Bruker Apex Kappa Duo with an Oxford Cobra Cryosystem low temperature device at 100(2) K using a MiTeGen micromount and NVH immersion oil. See Table S1 for crystal data and structure refinement details.

Bruker APEX¹ software was used to collect and reduce data and correct for Lorentz and polarization effects. Data were corrected for absorption effects using the Multi-Scan method SADABS.² Structures were solved with the SHELXT³ structure solution program using Intrinsic Phasing and refined using Least Squares method on F^2 with SHELXL⁴ within the OLEX2⁵ package. All non-hydrogen atoms were refined anisotropically. Hydrogen atoms were placed in calculated positions with Uiso dependencies derived from their carrier atoms (riding model).

¹ Bruker (2017). APEX3, Bruker AXS Inc., Madison, WI, USA.

² SADABS: Krause, L., Herbst-Irmer, R., Sheldrick, G. M., Stalke, D. (2015). *J. Appl. Cryst.* 48, 3-10.

³ Sheldrick, G. M. (2015). *Acta Cryst.* A71, 3-8

⁴ Sheldrick, G. M. (2015). *Acta Cryst.* C71, 3-8.

⁵ OLEX2: Dolomanov, O.V., Bourhis, L.J., Gildea, R.J., Howard, J.A.K. & Puschmann, H. (2009), *J. Appl. Cryst.* 42, 339-341.

In **1** the azide group is disordered and modelled over two locations (75:25% occupancy) and refined using geometric (SADI, DFIX) and displacement (SIMU, ISOR) restraints. The methanol OH hydrogen was located on the difference map and refined using geometric restraints (DFIX).

Crystallographic data have been deposited with the Cambridge Crystallographic Data Centre as supplementary publication no. 2296496. Copies of the data can be obtained, free of charge, on application to CCDC, 12 Union Road, Cambridge CB2 1EZ, UK, (fax: +44-(0)1223-336033 or e-mail:deposit@ccdc.cam.ac.uk).

Table S1. Crystal data and structure refinement for **1**

Identification code	TCD1950
CCDC No.	2296496
Empirical formula	C ₁₄ H ₁₈ ClN ₇ O ₄ Pt
Formula weight	578.89
Temperature (K)	100(2)
Crystal system	Monoclinic
Space group	P2 ₁ /n
a (Å)	14.8299(10)
b (Å)	7.2741(5)
c (Å)	17.2890(12)
α (°)	90
β (°)	96.980(3)
γ (°)	90
Volume (Å ³)	1851.2(2)
Z	4
ρ _{calc} (cm ³)	2.077
μ (mm ⁻¹)	15.846
F(000)	1112.0
Crystal size (mm ³)	0.106 × 0.074 × 0.018
Radiation	Cu Kα (λ = 1.54178)
2θ range for data collection (°)	7.422 to 140.21
Reflections collected	21407
Independent reflections	3482
	R _{int} = 0.0602
	R _{sigma} = 0.0485
Data/restraints/parameters	3482/89/278
Goodness-of-fit on F ²	1.141
Final R indexes [I ≥ 2σ (I)]	R ₁ = 0.0322, wR ₂ = 0.0835
Final R indexes [all data]	R ₁ = 0.0394, wR ₂ = 0.0873
Largest diff. peak/hole (e Å ⁻³)	1.07/-1.16

Table S2. Crystal data and structure refinement for **1**.

Identification code	TCD1950
CCDC No.	2296496
Empirical formula	C ₁₄ H ₁₈ ClN ₇ O ₄ Pt
Formula weight	578.89
Temperature (K)	100(2)
Crystal system	Monoclinic
Space group	P2 ₁ /n
a (Å)	14.8299(10)
b (Å)	7.2741(5)
c (Å)	17.2890(12)
α (°)	90
β (°)	96.980(3)
γ (°)	90
Volume (Å ³)	1851.2(2)
Z	4
ρ _{calc} (cm ³)	2.077
μ (mm ⁻¹)	15.846
F(000)	1112.0
Crystal size (mm ³)	0.106 × 0.074 × 0.018
Radiation	Cu Kα (λ = 1.54178)
2θ range for data collection (°)	7.422 to 140.21
Reflections collected	21407
Independent reflections	3482 R _{int} = 0.0602 R _{sigma} = 0.0485
Data/restraints/parameters	3482/89/278
Goodness-of-fit on F ²	1.141
Final R indexes [I ≥ 2σ (I)]	R ₁ = 0.0322, wR ₂ = 0.0835
Final R indexes [all data]	R ₁ = 0.0394, wR ₂ = 0.0873
Largest diff. peak/hole (e Å ⁻³)	1.07/-1.16

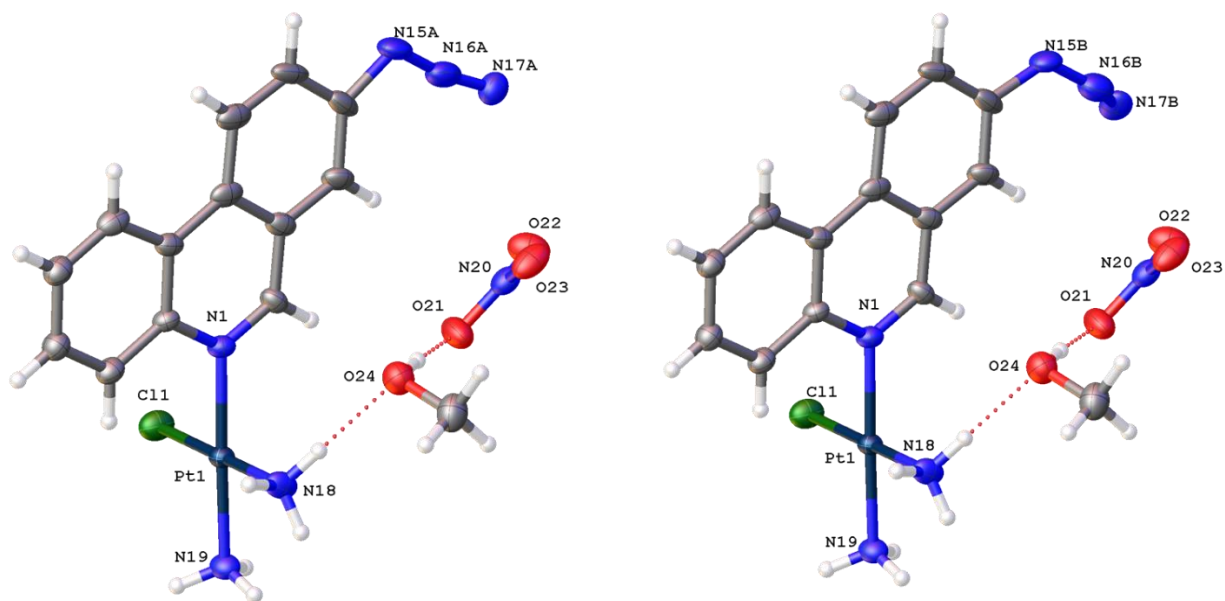


Figure S12. Individual images of each disordered moiety of **1** with (A) 75% occupied and (B) 25% occupied. Atomic displacement shown at 50% probability and heteroatoms labelled only.

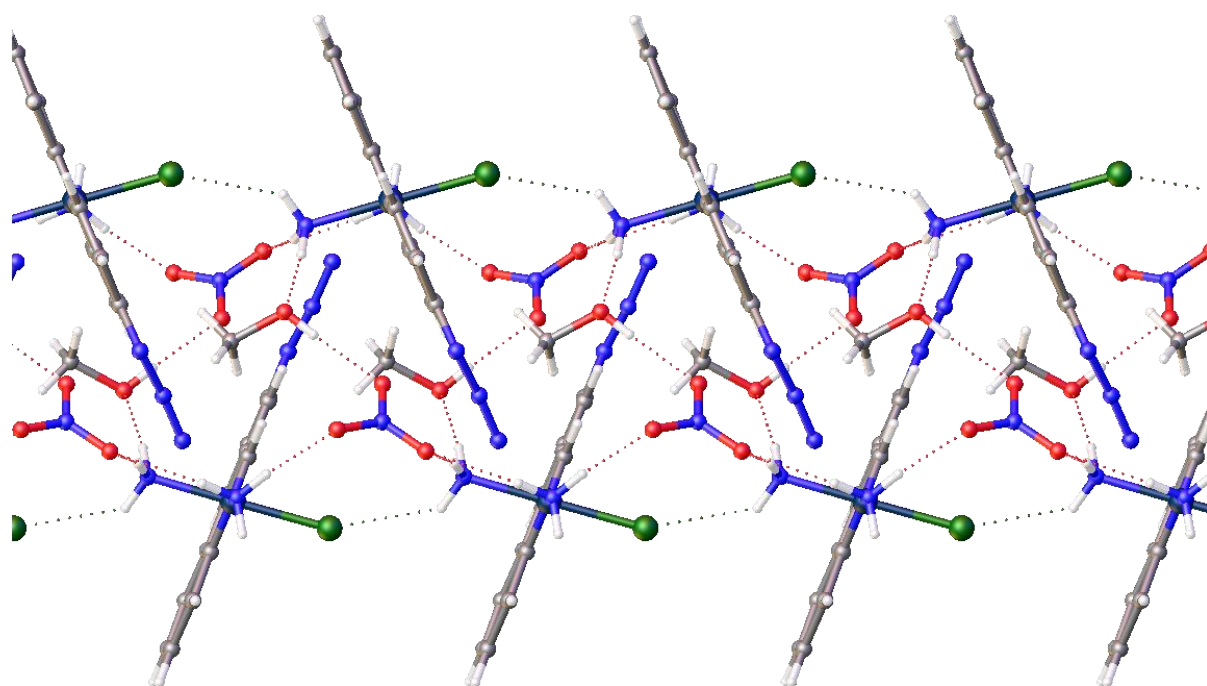


Figure S13. Strong hydrogen bonding network in **1** viewed normal to the *c*-axis. Hydrogen bonding represented by dotted lines. Atomic displacement shown at 50% probability.

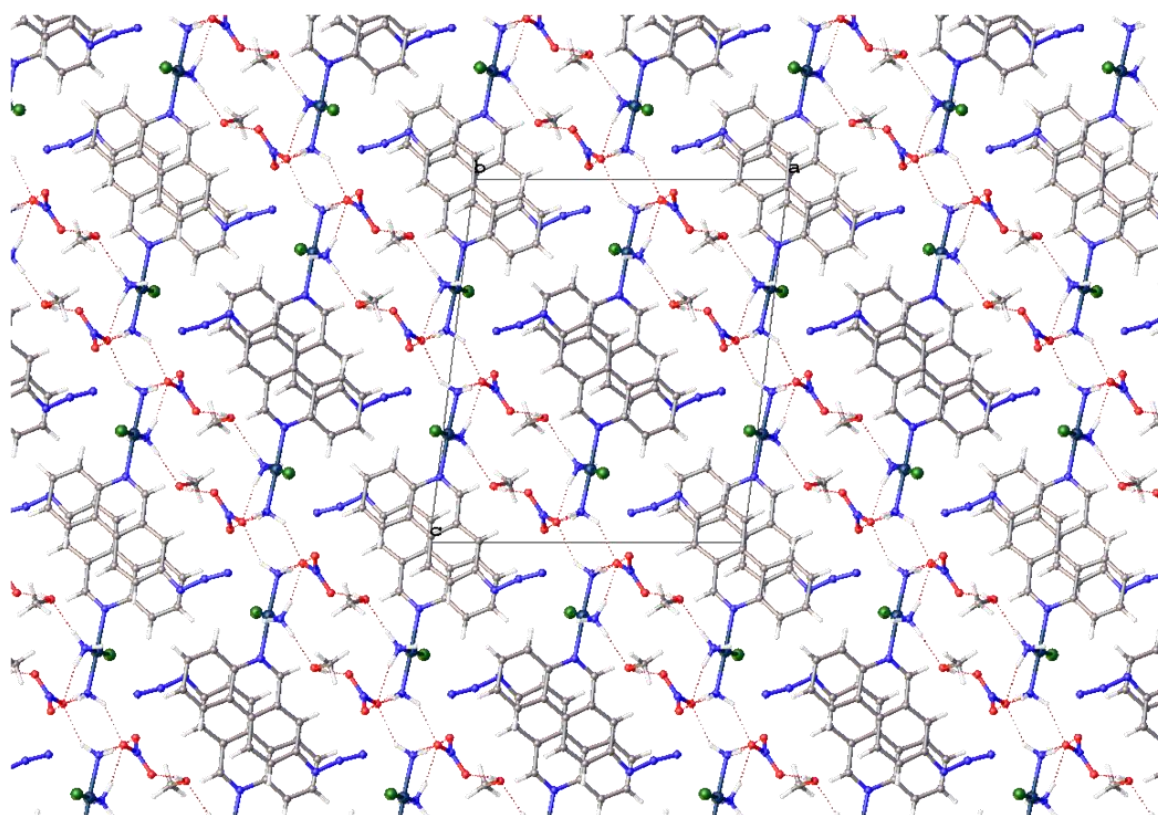


Figure S14. Schematic packing diagram of the major occupied moiety in **1** viewed normal to the b-axis. Dotted lines indicate hydrogen bonding interactions.

Table S3. Hydrogen Bonds for **1**.

D	H	A	d(D-H)/Å	d(H-A)/Å	d(D-A)/Å	D-H-A/°
N18	H18A	O24	0.91	1.96	2.862(6)	174
N18	H18B	O23 ¹	0.91	2.08	2.978(6)	167
N19	H19A	O22 ²	0.91	2.10	2.999(6)	171
N19	H19B	O23 ³	0.91	2.38	3.087(7)	134
N19	H19C	O23 ¹	0.91	2.29	3.192(6)	169
O24	H24	O21	0.842(10)	1.959(16)	2.796(6)	172(7)

¹1/2-X, -1/2+Y, 3/2-Z; ²1/2-X, 1/2+Y, 3/2-Z; ³1/2+X, 3/2-Y, 1/2+Z

Table S4. Bond lengths (Å) and Angles (°) for **1**, phenanthriplatin and the triflate derivative

	1	phenanthriplatin	triflate

Pt1-Cl1	2.2946(14)	2.2998(19)	2.2962(7)
Pt1-N1	2.045(5)	2.032(6)	2.047(2)
Pt1-N18	2.043(4)	2.040(6)	2.025(2)
Pt1-N19	2.047(5)	2.036(6)	2.039(2)
N1-Pt1-Cl1	91.70(12)	85.90(18)	87.72(6)
N1-Pt1-N19	178.28(18)	176.4(2)	177.97(9)
N18-Pt1-Cl1	179.31(15)	178.26(19)	179.31(6)
N18-Pt1-N1	88.58(17)	94.2(3)	92.96(9)
N18-Pt1-N19	91.57(18)	89.4(3)	89.05(9)
N19-Pt1-Cl1	88.13(13)	90.51(19)	90.27(6)

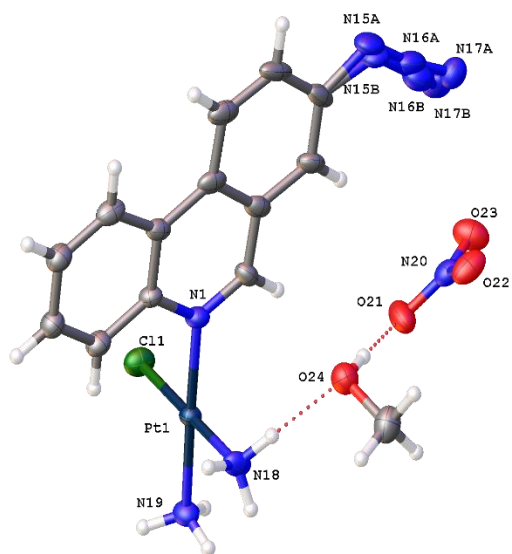


Figure S15. Disordered molecular structure of 1, showing the NO_3^- counter ion and MeOH solvate. Atomic displacement shown at 50% probability and heteroatoms labelled only.

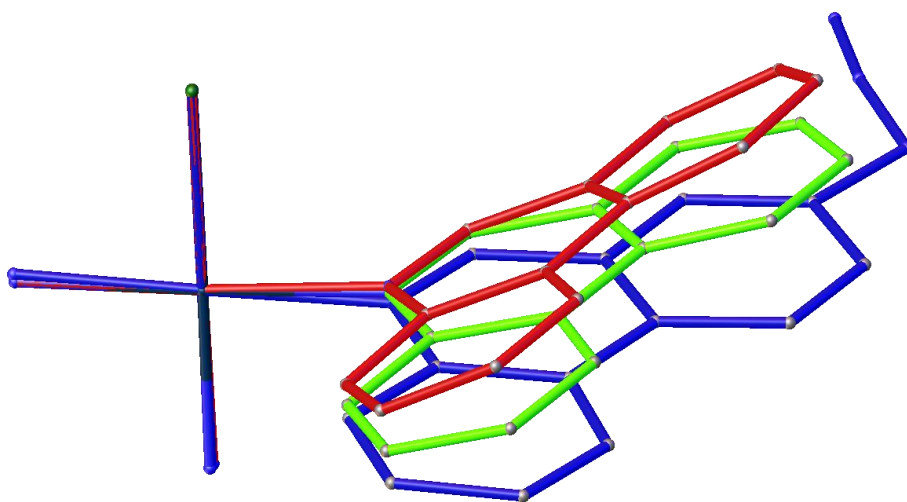


Figure S16. Overlay of **1** (Blue), triflate salt of phenanthriplatin (Green) and nitrate salt of phenanthriplatin (Red).

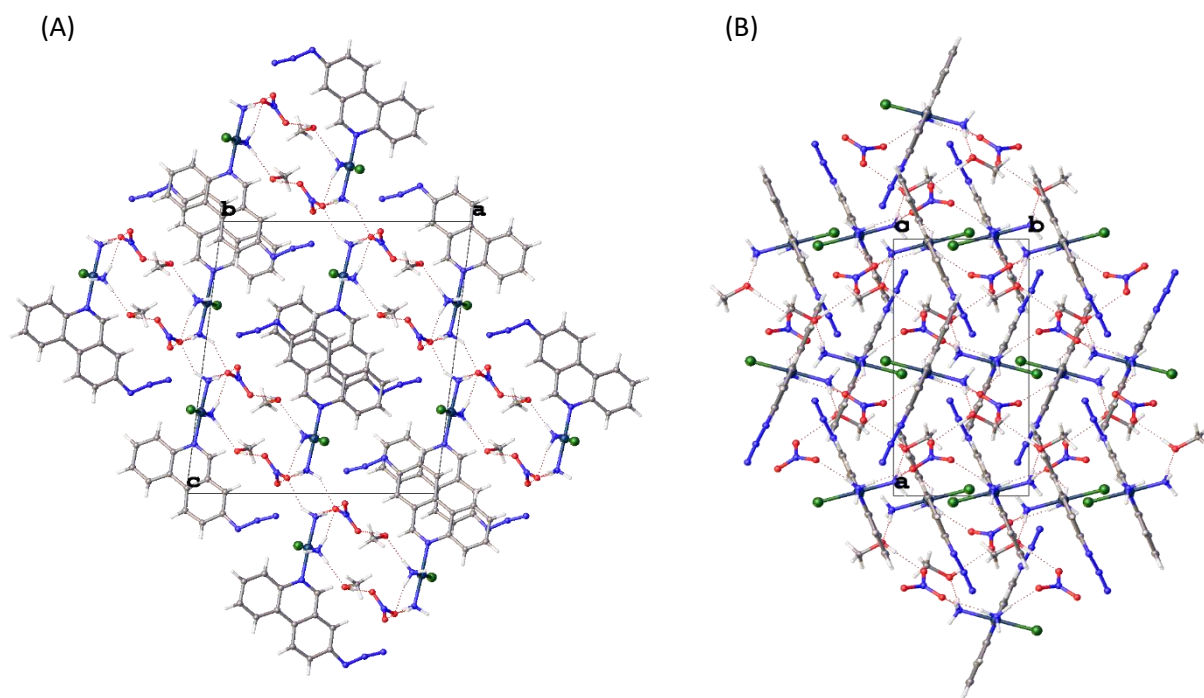


Figure S17. Schematic packing diagrams of **1** showing the π - π stacking viewed (A) normal to the B-axis and (B) normal to the c-axis. Dotted lines indicate hydrogen bonding interactions.